A Comparison of a GCM Simulation of the Seasonal Cycle of the Atmosphere With Observations Part II: Stationary Waves and Transient Fluctuations

David M. Straus
Laboratory for Atmospheres
NASA/Goddard Space Flight Center
Greenbelt, MD 20771
and
J. Shukla
Center for Ocean-Land-Atmosphere Interactions
Department of Meteorology
University of Maryland
College Park, MD 20742

[Original manuscript received 16 June 1987; in revised form 22 April 1988]

ABSTRACT *This paper presents the seasonal dependence of the stationary and transient eddies of the GLAS/UMD GCM from a two-year annual cycle integration.*

The simulated Northern Hemisphere stationary waves are realistic in winter (below 250 mb) and in spring and fall; in winter a large anomalous ridge over the date-line is noted above 250 mb. The model does not simulate the winter barotropic trough over eastern Canada. In summer the mid-latitude stationary waves are poorly simulated (possibly owing to anomalous summer rainfall), but the monsoonal structure in the tropics is captured.

The stationary wave field at 500 mb in the Southern Hemisphere is not well simulated, with the range of season-to-season variability being much larger than observed. The zonally averaged stationary wave rms is realistic below 200 mb in winter and spring, but is less so in summer and autumn, possibly due to erroneous summertime precipitation.

The geographical distributions of 500-mb transient and band-pass height rms, of transient 850-mb heat flux and of 200-mb momentum flux in the Northern Hemisphere are well simulated except for summer. The latitude-height dependence of height rms and low-level transient heat flux is realistic in both summer and winter, but the transient momentum flux is not well simulated in summer. The mid-level transient heat flux is too strong.

The overall pattern of transient activity at 500 mb in the Southern Hemisphere is reasonable in the GCM, although there is too much variability in the eastern Pacific, while the observed peak in rms in the New Zealand sector is displaced eastwards in the GCM. The latitude-height

dependence of transient height rms and transient fluxes of heat and momentum looks quite realistic, and is similar in accuracy to the Northern Hemispheric results.

RÉSUMÉ *On présente la dépendance saisonnière des tourbillons stationnaires et transitoires du modèle de circulation générale (MCG), du Goddard Laboratory of Atmospheric Sciences (GLAS) à l'Université du Maryland, d'une intégration annuelle d'un cycle de deux ans.*

Les ondes stationnaires simulées dans l'hémisphère Nord sont réalistes en hiver (sous 250 mb) et au printemps et en automne; en hiver, on peut noter une forte crête anormale au-dessus de la ligne de changement de jour (au-dessus de 250 mb). Le modèle ne simule pas le creux barotropique hivernal au-dessus de l'est du Canada. Les ondes stationnaires des latitudes moyennes sont pauvrement simulées en été (les anomalies de précipitation estivale pourraient en être la cause), mais la structure des moussons dans les tropiques est évidente.

Le champ d'ondes stationnaires à 500 mb n'est pas bien simulé au-dessus de l'hémisphère Sud; la variabilité de saison en saison étant beaucoup plus grande que celle observée. La moyenne quadratique (MQ) de l'onde stationnaire en chaque zone est réaliste sous 200 mb en hiver et au printemps, mais moins en été et en automne, probablement à cause des précipitations estivales erronées.

La distribution géographique de la MQ des hauteurs transitoire et de la passe-bande à 500 mb, du flux thermique transitoire à 850 mb, et du flux de quantités de mouvement à 200 mb dans l'hémisphère Nord est bien simulée, sauf en été. La dépendance latitude-hauteur de la MQ des hauteurs et du flux thermique transitoire à basse altitude est réaliste en été et en hiver; cependant, le flux transitoire de quantités de mouvement n'est pas bien simulé en été. Le flux thermique transitoire à moyenne altitude est trop fort.

Dans l'hémisphère Sud, le MCG présente une configuration générale satisfaisante de l'activité transitoire à 500 mb, même s'il y a trop de variabilité dans l'est du Pacifique, lorsque la valeur maximale de la MQ observée dans la région de la Nouvelle-Zélande est déplacée vers l'est dans le modèle. La dépendance latitude-hauteur de la MQ de la hauteur transitoire et des flux transitoire et de quantités de mouvement semble bien réaliste et son exactitude est semblable aux résultats pour l'hémisphère Nord.

1 Introduction

This paper constitutes the second part of a two-part study of the simulation of the seasonal cycle with the GLAS/U of MD Climate general circulation model (GCM). The mean fields and annual harmonics resulting from a two-year integration of the model are described in Part I (Straus and Shukla, 1988, hereafter referred to as SS1). The energy cycle is discussed by Straus (1988). As emphasized in SS1, our ability to use GCMs effectively in the understanding and prediction of interannual variability and long-term climate change requires that the models be able to accurately simulate the seasonal cycle. Accordingly, the main goal of this study is to compare the GCM's seasonal cycle with observations and with the published results of other GCMs in a critical way.

While SS1 concentrated on the annual harmonics and on the mean fields, this paper discusses the stationary and transient disturbances. We compare the simulated eddy statistics of the GLAS GCM with those of the Community Climate Model (CCM) simulations of perpetual winter and summer (Malone et al., 1984, hereafter referred to as M), recognizing that the CCM (an R15 spectral model) has a slightly coarser resolution than the GLAS GCM, and that there may be significant differences between annual cycle and perpetual integrations with any GCM (Zwiers and Boer, 1987). (For a brief review of previous work on the simulation of the seasonal cycle, see SS1.)

The Northern Hemispheric stationary and transient eddies are more realistic in winter than in summer in both the GLAS GCM and the NCAR CCM. In addition, the geographical dependence of the stationary waves is more realistic in the Northern than in the Southern Hemisphere. These similarities occur despite fairly large differences in the simulation of the upper troposphere, where the zonally averaged temperature and wind fields are more realistic in the CCM. We suggest that the seasonal dependence in both models is due to their difficulty in correctly simulating summer precipitation (see SS1). The CCM suffers the additional problem that "The transient eddies in both summer hemispheres are much too weak" (Malone et al., 1984). This is not the case for the GLAS GCM, for here both the transient height variance and heat flux (but not momentum flux) in the northern summer have the correct overall magnitudes, and the Southern Hemisphere summer transient eddies are realistically vigorous.

The GLAS/UMD GCM itself is discussed in detail in SS1, along with the initial and boundary conditions used in the integration.

Section 2 describes the data base and the analysis procedures, while Sections 3 and 4 discuss the stationary waves for the Northern and Southern Hemispheres, respectively. The transient fluctuations for the two hemispheres are presented in Sections 5 and 6, and a discussion is given in Section 7.

2 Data sets and analysis procedures

a *GCM Simulation*

The GCM was integrated for a two-year period, with the boundary conditions of solar insolation, sea surface temperature, sea-ice extent and soil moisture prescribed to follow a smooth seasonal cycle determined from climatology. The model was initialized with data valid for 15 November 1978. The data used in this study consist of the model output, stored for two times each day (00 and 12 UTC) and interpolated to pressure surfaces, for the period 1 December 1978 to 30 November 1980, inclusive, where the significance of the year is only in the time elapsed after that of the initial conditions. For further details concerning the GCM and the integration, see SS1.

b *Observed Data*

The atmospheric analyses with which we compare the model results are described in detail in SS1; here we only list them briefly: (i) the 14½-year set of National Meteorological Center (NMC) analyses covering 1 June 1963 to 31 December 1977 from 22 to 90°N; (ii) the 11-year set of 500-mb height analyses of the Australian Bureau of Meteorology spanning the period from 1 June 1972 to 31 May 1983, from 10 to 90°S; (iii) the European Centre (ECMWF) global analyses of the year of the GWE, 1 December 1978 to 30 November 1979; and (iv) the 7-year set of European Centre global analyses (ECMWF-7) from 1 January 1980 to 31 December 1986.

c *Analysis Methods*

The definition of the stationary eddies ("stationary waves") in this paper is very similar to that used in Lau (1979b): The stationary eddy field is the departure from the zonal mean, averaged over season. The seasons used in this paper are (i) Dec.–Feb. (DJF); (ii) Mar.–May (MAM), (iii) June–Aug. (JJA) and (iv) Sept.–Nov. (SON). The seasonal averages of the eddy component were further averaged over the number

of equivalent seasons in each data set (two for the GCM, seven for the ECMWF-7 analyses, etc.) to obtain the final seasonal mean stationary eddy field. Zonally averaged eddy variances and covariances (such as $[\bar{z}^{*2}]$, $[\bar{v}^*\bar{T}^*]$, etc.) were calculated directly from the final seasonal mean stationary eddy fields[1]. The method used here of calculating (co)variances is not identical to calculating the (co)variances separately for each equivalent season and then averaging, but the difference in the final statistics between the two methods is expected to be less than 10% (Lau, 1979b).

The transient variances and covariances (such as $\overline{(z'^2)}$, $\overline{(v'T')}$, etc.) were computed by (i) obtaining the seasonal time series of all relevant variables at the appropriate pressure levels for all grid points, (ii) removing the annual mean and annual and semi-annual harmonics, (iii) time-filtering the time series with a "low-pass" and "band-pass" filter, (iv) calculating the local (co)variances from both the filtered and unfiltered series for each season and (v) averaging over equivalent seasons in each data set. The low-pass filter used here has the same frequency response as that of Blackmon (1976), retaining periods between 10 and 90 d, excluding the seasonal cycle. The band-pass filter frequency response is identical to that of Blackmon and White (1982), retaining periods of between approximately 2.5 and 10 d. (The actual process of time filtering used in this paper was slightly different from that used by both Blackmon (1976) and Blackmon and White (1982), who used filters defined by a set of running means over the original data. Here we directly computed the discrete time Fourier spectrum of each time series (after the removal of the seasonal cycle), multiplied it by the (discrete) response function, and resynthesized the filtered series.)

3 Northern Hemisphere stationary eddies

a *The 200-mb Geopotential Height*

The observed winter (DJF) stationary eddy height field $\bar{z}^*$ at 200 mb (Fig. 1a) is dominated by strong minima over Eastern Canada and the East Coast of Asia (corresponding to troughs in the total time-averaged height fields in these areas) and maxima over the mid-latitude eastern oceans (corresponding to ridges). Also note the extension of the Asian minimum westward all the way to the Atlantic Ocean and the secondary minimum over Africa. There is a distinct change of phase in all these features near 30°N, since the eddy pattern changes sign there.

The primary observed change in going from winter to spring is a weakening of the main features (Fig. 1b). Some changes of morphology occur, however; the maximum over the eastern Pacific becomes very diffuse, whereas that over the eastern Atlantic extends into central Asia, isolating the minimum over Africa. The summer pattern (Fig. 1c) shows a large change, with maxima (ridges) over the central portions of North America and Asia and tilted minima (troughs) over the subtropical oceans. At higher latitudes, the prominent features are a minimum over eastern Canada (located

[1]Our notation is standard: An overbar represents the seasonal time mean, a prime denotes a deviation from that mean, brackets denote a zonal mean, and a star the deviation from the zonal mean. In certain cases, a prime denotes the result of further temporal filtering after removal of the mean. It will be clear from the context which meaning is being used.

slightly eastward of its winter position) and one over the Bering Sea, and maxima over western Russia and over Siberia.

The transition from summer to fall is dramatic (Fig. 1d), for the fall pattern is similar to that of winter. In the subtropics, the distinct change in phase of the eddies near 30°N, which was lost in summer, is re-established in fall.

The GCM's stationary eddy field $\bar{z}^*$ at 200 mb in winter (Fig. 2a) is similar to the observations' except that the observed eastern Pacific maximum is shifted eastward to western North America, and the observed minimum over eastern Canada completely disappears. (The maximum to the west of the United Kingdom is also too weak in the GCM result.) As in nature, the GCM weakens most of the main features of the eddy field in spring (Fig. 2b). The anomalously shifted maximum over western North America does not weaken enough, however, and the lack of an eastern Canadian minimum is still seen. The observed extension of a positive region into central Asia is exaggerated by the GCM.

The summer pattern (Fig. 2c) represents a marked change in the GCM's eddies, which also occurs in nature. The overall appearance of the field is realistic only in the sense that the minima are over the oceans and the maxima over the land. The observed, fairly localized ridge in the mid-latitude central Atlantic is completely missing in the simulated results, so that the eastern Canadian minimum (which the GCM now does show) extends across the north Atlantic and into western Europe. Other unrealistic features of the simulation are the extreme amplitudes of the eddy field over central Asia and Africa and the lack of a distinction between the tropical and high-latitude minima in the Pacific Ocean.

A direct comparison with the stationary eddy fields of the CCM is obscured slightly because M show only the total 300-mb height field (their Figs 4 and 6 for northern winter and summer, respectively), but it is clear that the summer simulation is the poorer. Errors in the mean summer height map include excessively deep troughs in both the Pacific and Atlantic, leading to large negative stationary eddy anomalies there. The Pacific anomaly in the CCM is located 30° eastward of a similar negative anomaly in the GLAS GCM (Fig. 2c).

While the fall pattern of $\bar{z}^*$ in nature is quite similar to that in winter (but with lesser amplitude), this is not true in the GCM (Fig. 2d). For example, the minimum (trough) over the east Asian coast is shifted considerably, in addition to being much less intense than in winter. Also, the maximum over western North America shifts by 30° longitude between fall and winter, a greater shift than that observed.

b *Vertical Structure*

The vertical structure of the stationary waves may be viewed from longitude-height sections of the stationary eddy height ($\bar{z}^*$) and temperature ($\bar{T}^*$) fields at various latitudes. Winter sections of the observed (NMC) $\bar{z}^*$ at 46 and 26°N are shown in Figs 3a and b, and sections of $\bar{T}^*$ in Figs 3c and d. The corresponding GCM results are given in Figs 3e–h. The observed winter sections of $\bar{z}^*$ at 26 and 46°N are quite similar to those discussed by Lau (1979b), having a vertical structure that is characterized by a distinct westward tilt with height at 46°N, and by less tilt at 26°N. The wave amplitude reaches a peak near the tropopause at 26 and 46°N, but continues to

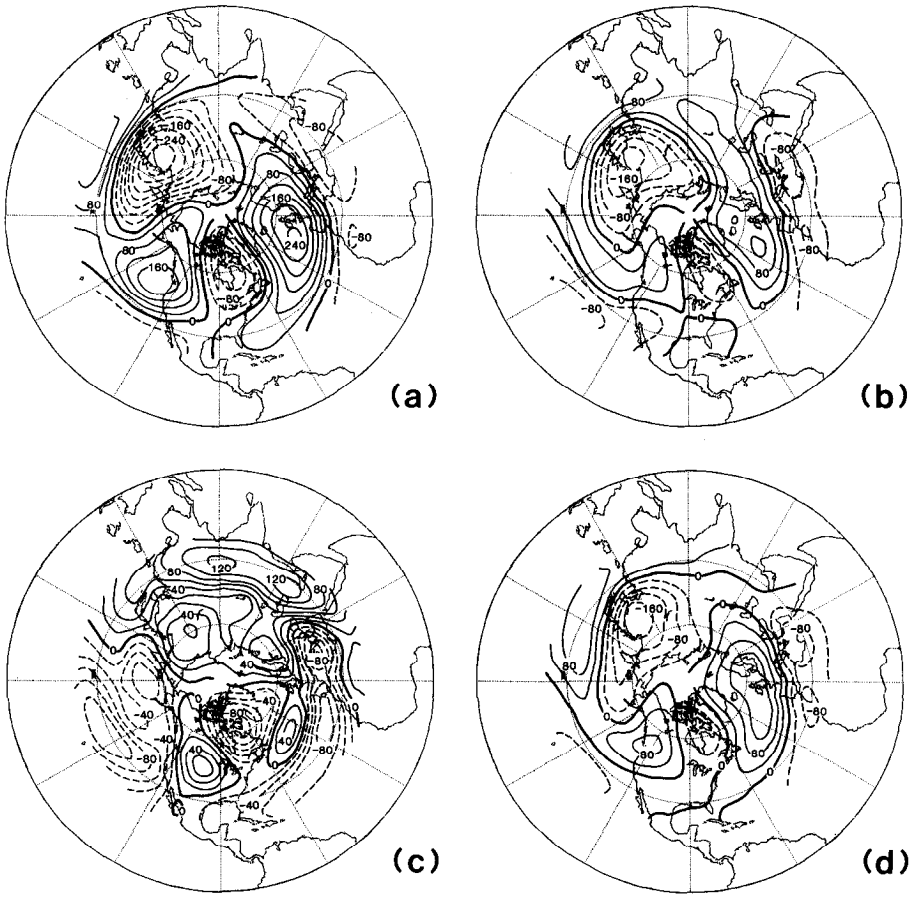

Fig. 1 Stationary eddy component of the 200-mb height field from NMC data for the Northern Hemisphere: (a) winter (DJF), (b) spring (MAM), (c) summer (JJA) and (d) fall (SON). Contour interval: 40 m for (a), (b) and (d); 20 m for (c).

increase into the stratosphere at higher latitudes (not shown). A comparison of the fields for 26 and 42°N shows the phase reversal mentioned in the previous subsection. The corresponding temperature field $\tilde{T}^*$ is closely tied to the underlying topography in middle and high latitudes (Lau, 1979b), with the coldest air lying over the eastern coasts of North America and Asia and the warmest air over the west coasts.

Although the vertical structure of the winter stationary eddies in the GCM is generally realistic below 300 mb, there are some striking discrepancies in comparison with observations, especially at upper levels. The eddies do not peak in amplitude near the tropopause, but rather increase up to 100 mb at all latitudes. Furthermore, the observed (gradual) westward tilt with height of the ridge over western North America and the eastern Pacific at 46°N is not captured by the GCM below 200 mb, whereas a large positive anomaly occurs in the GCM over the date-line at 100 mb. The eastern Canadian minimum, so evident in the observations at all levels in mid- and high

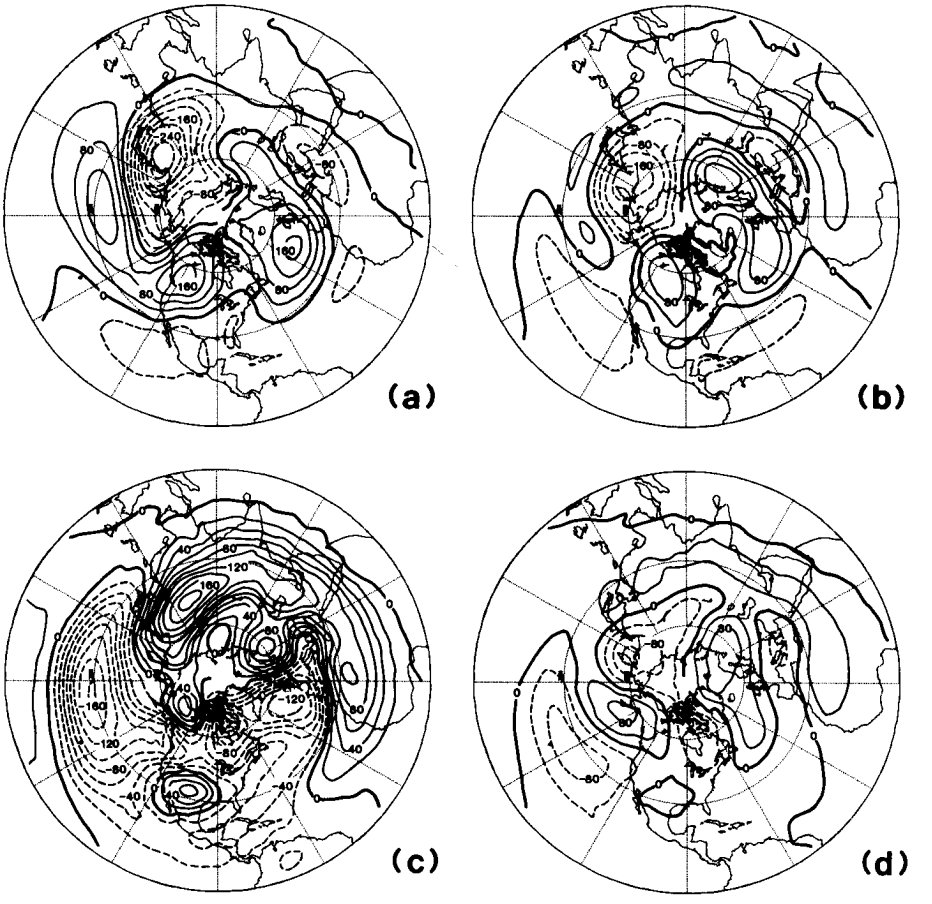

Fig. 2 As Fig. 1, except for the GCM data.

latitudes, is very weakly represented by the GCM except for 100 mb near 46°N. These discrepancies also manifest themselves in the temperature field. In the subtropics, the observed out-of-phase relationship between the upper troposphere and stratosphere is completely missing in the GCM results. Whereas the low-level eddy field at 46°N and at higher latitudes in the GCM is similar in most respects to the observed, the low-level temperatures over North America are significantly too high.

The observed vertical structure of the $\bar{z}^*$ field in spring (not shown) is remarkably similar to that in the winter season, only with a reduction in amplitude and in westward phase tilt. The transition to summer is accompanied (in nature) by a further weakening of the stationary waves in mid- and high latitudes and by the absence of any noticeable phase tilt with height. In the summer subtropics (Fig. 4b), the vertical structure of $\bar{z}^*$ exhibits clear evidence of monsoonal behaviour, with the upper and lower levels having opposite phases. The subtropical temperature field now shows an out-of-phase relationship between the troposphere and stratosphere, and the low-level temperature pattern in mid-latitudes has shifted from its winter configuration, so that

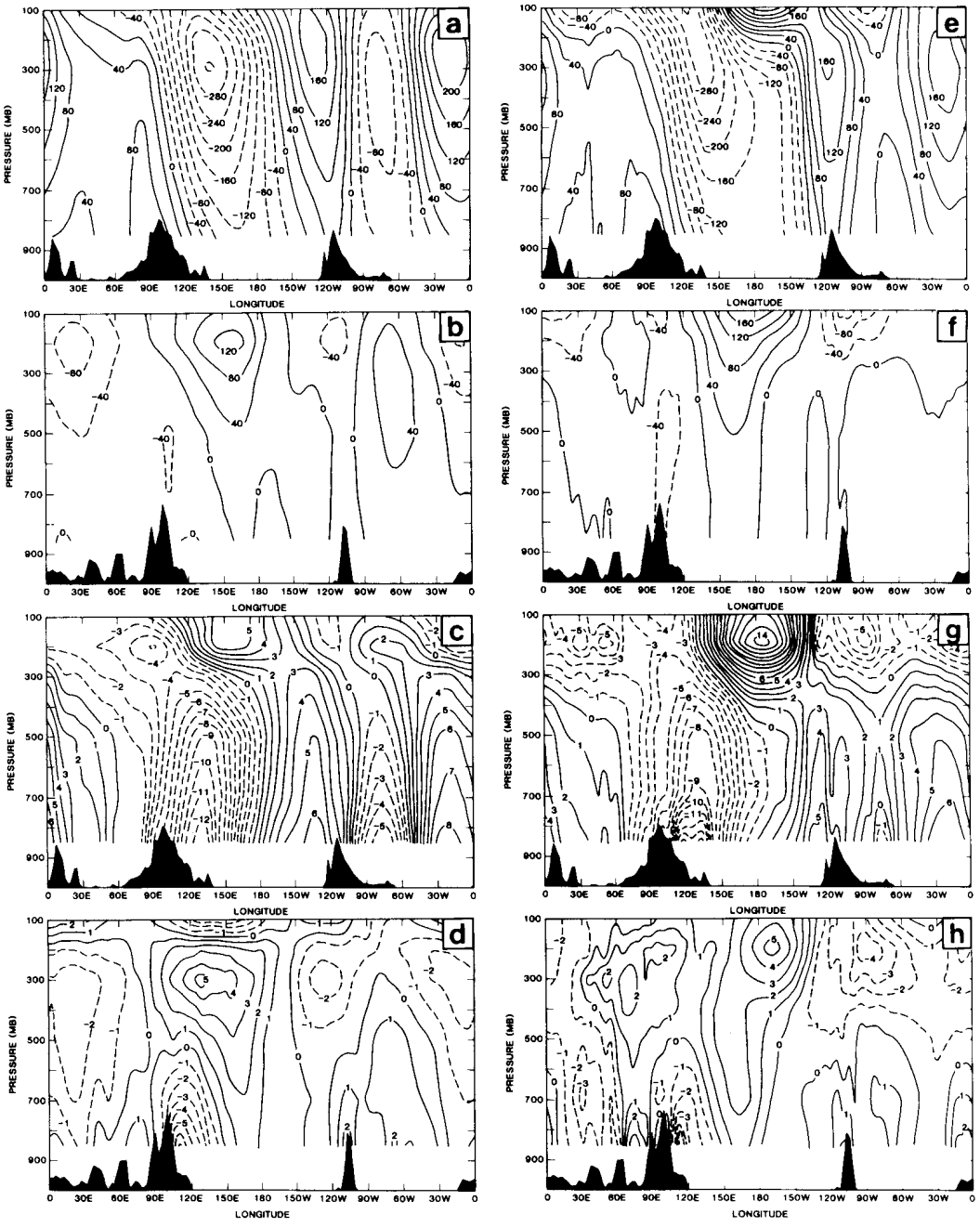

Fig. 3 Longitude-pressure sections of the stationary eddy fields during the northern winter (DJF). (a) $\bar{z}^*$ at 46°N from NMC data, (b) $\bar{z}^*$ at 26°N from NMC data, (c) $\bar{T}^*$ at 46°N from NMC data, (d) $\bar{T}^*$ at 26°N from NMC data, (e) $\bar{z}^*$ at 46°N from GCM data, (f) $\bar{z}^*$ at 26°N from GCM data, (g) $\bar{T}^*$ at 46°N from GCM data and (h) $\bar{T}^*$ at 26°N from GCM data. Contour intervals: 40 m (height): 1 K (temperature).

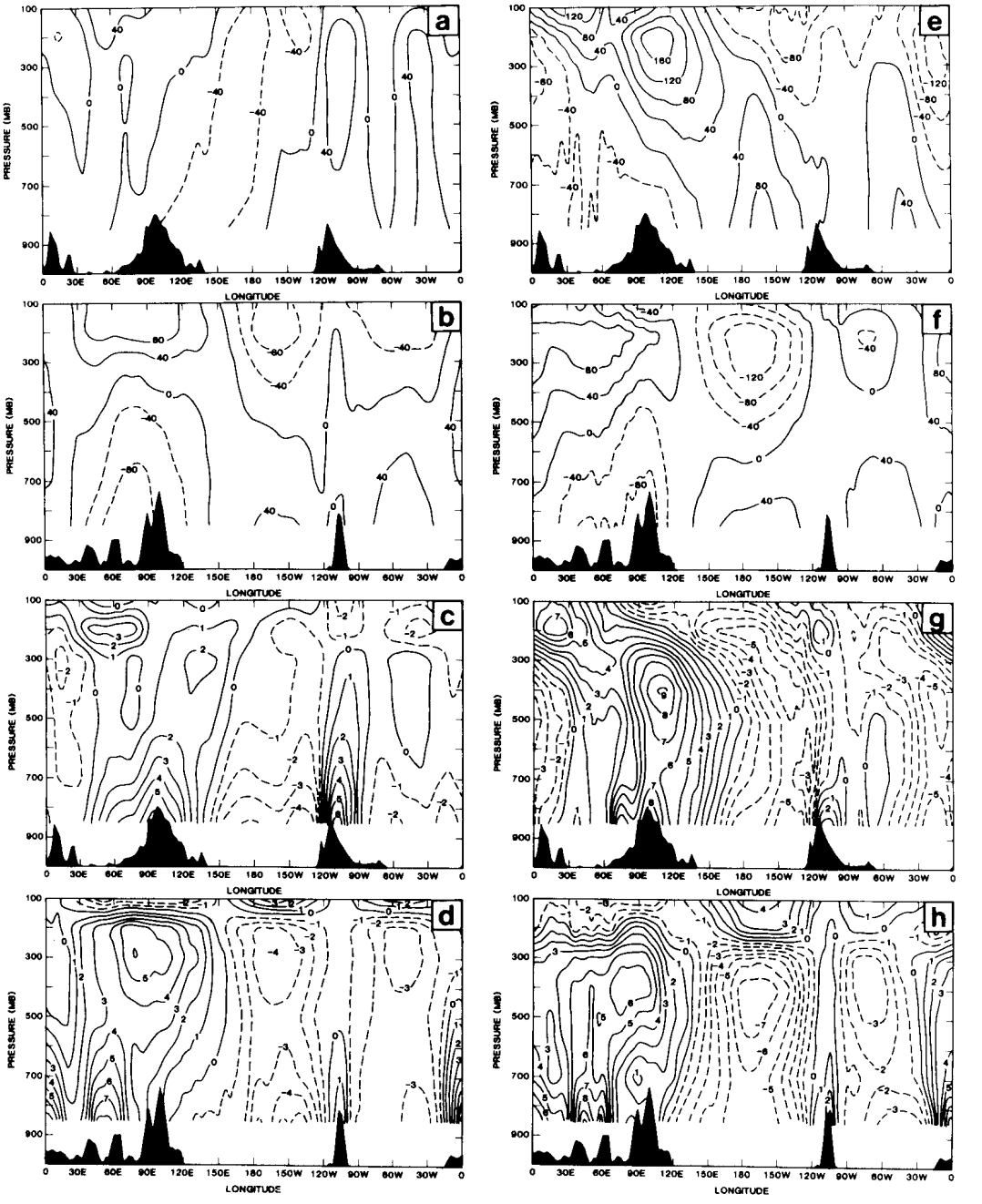

Fig. 4 As Fig. 3, except for the northern summer (JJA).

the warmest air now lies over central North America and Asia. The overall vertical structure of the observed stationary waves in fall is almost identical to that of winter, but (again) with a smaller amplitude (not shown). Thus in terms of the stationary eddy *structure* it is the summer that stands out as the unique season.

Although the vertical structure of the GCM's stationary eddy height field in spring (not shown) shows little change from winter at high latitudes, there is a significant change in mid-latitudes, where the large positive anomaly at 100 mb over the date-line disappears in spring. The vertical configuration at 26°N in spring also becomes more realistic, with 200 mb now becoming the level of maximum amplitude. In terms of overall vertical phase shift, the GCM spring results appear to be fairly realistic. However, the simulation continues to underpredict the eastern Canadian minimum at mid- and high latitudes.

In the summer, the GCM's $\bar{z}^*$ field appears most realistic at 26°N, where most of the observed features are well reproduced indicating monsoonal behaviour in the GCM. At 46°N and higher latitudes (not shown), the summer simulation has serious problems. Not only are the wave amplitudes far too large, but they also show more westward phase tilt with height than that observed. The upper-level minimum over the Atlantic at 46°N is completely out of phase with the observations. At lower levels, the simulation is improved in that warm air correctly lies over the continents.

The fall pattern simulated by the GCM (not shown) shows many similarities to the GCM winter results at 46°N and higher latitudes, but the eddies have a smaller amplitude in fall, as is observed. In fact, at all latitudes, the GCM fall results are more realistic than those of winter, including a reasonable fall simulation of the eastern Canadian minimum and the absence of the winter mid-latitude anomaly at 100 mb. This realism of the fall stationary eddies is also seen in the temperature field.

c *Zonally Averaged Statistics*

A measure of the overall strength of the stationary eddies is afforded by zonally averaging various stationary eddy variances and covariances. The root mean square (rms) of the geopotential height $[\bar{z}^{*2}]^{1/2}$ is given for each of the four seasons for the NMC data in Figs 5a–d and for the GCM in Figs 5e–h. These figures clearly show the nature of the seasonal cycle of the rms height field. The winter-time maximum of rms at 50°N in the upper troposphere is present in both transition seasons (at about 60% of its winter-time value) and is shifted only slightly poleward. It is also present during summer, when it is quite weak and has moved to near 60°N. The subtropical maximum at 200 mb is present in all seasons, but it is relatively weak in winter, spring and fall. In summer, it is accompanied by a strong subtropical maximum at 850 mb. The subtropical maxima are manifestations in the zonal mean of the monsoonal features described earlier.

The GCM's rms eddy height field is realistic in that the observed winter-time maximum in mid-latitudes is present, and weakens (and moves polewards) in spring and fall. The upper-level subtropical maximum in rms during spring and fall and the monsoonal features in summer are reproduced. One feature of the winter simulation that is clearly anomalous is the increase in rms above 200 mb near 40°N, leading to very large values at 100 mb and completely obscuring the secondary subtropical

maximum at that level. Note that below 250 mb the winter simulation is realistic. The model clearly tends to produce eddy variances that increase continuously with height and do not weaken in the stratosphere, and this problem occurs in each season. Recalling from the previous paper (SS1) that the simulated subtropical jets increase right up to 100 mb in the GCM in all seaons (so that the observed negative shear in $[u]$ in the lower stratosphere is not simulated), we suggest that the anomalous increase in stationary eddy strength with height is intimately related to the corresponding behaviour in $[u]$. In addition to being vertically displaced, the GCM summer mid-latitude maximum is far too intense, whereas during spring and fall it is displaced too far polewards.

The winter latitude-height section of $[\bar{z}^{*2}]^{1/2}$ for the CCM (Fig. 3 of M) is quite comparable to Fig. 5e below about 200 mb. Above this, the CCM simulation is clearly superior, consistent with the more realistic simulation of the polar night jet in the CCM (see SS1). The summer zonally averaged rms is also much more realistic at high latitudes in the upper troposphere in the CCM compared with that in Fig. 5g for the GLAS GCM. However, simulating the correct amount of variance does not always guarantee an accurate geographical pattern, as indicated in the previous section.

The stationary eddy fluxes of heat ($\bar{v}^*\bar{T}^*$) and momentum ($\bar{u}^*\bar{v}^*$) depend on both the amplitudes and the vertical and horizontal phase shifts (respectively) of the stationary waves. The westward tilt with height evident in the observed winter-time $\bar{z}^*$ field in mid-latitudes is reflected in the strong winter eddy heat flux, with maximum fluxes occurring at both upper and lower levels (Fig. 6a). The reduced amplitude and tilt of the $\bar{z}^*$ field in the transition seasons combines to give a reduced heat flux during these seasons, although the overall structure remains similar to that in winter with the exception of a slight poleward shift. The virtual absence of any phase shift in mid- and high latitudes in summer is responsible for the weakness of the heat flux there. A weak summertime maximum does occur near 38°N at 300 mb.

The GCM winter stationary eddy heat flux (Fig. 6e) is quite realistic, both in terms of magnitude and overall structure. The only level at which the simulation is noticeably different from the observations is 100 mb, where the largest simulated values are located 10° too far equatorwards. Differences are found, however, in the behaviour of the simulated heat flux compared with the observations throughout the rest of the year. During the transition seasons, the GCM produces a maximum heat flux at 850 mb, in contrast to the observed upper tropospheric maxima. This is in part due to the tendency of the $\bar{z}^*$ field at high latitudes in the GCM to have its vertical tilt too low down in the atmosphere during these seasons. In summer the simulated upper-level stationary eddy heat flux is far too strong (by nearly a factor of 4), and also is shifted polewards of the observed location. This discrepancy is consistent with the overly vigorous simulated $\bar{z}^*$ field in summer at mid- and high latitudes (Fig. 4). The greater realism of the GCM $\bar{z}^*$ summer field at 26°N is also reflected in the heat flux, which correctly changes sign near 30°N.

The zonally averaged eddy momentum flux ($[\bar{u}^*\bar{v}^*]$) is a measure of both the amplitudes and horizontal phase shifts of the stationary waves. The well known observed dipole pattern in winter (Fig. 7a) reaches a maximum at 200 mb, with a

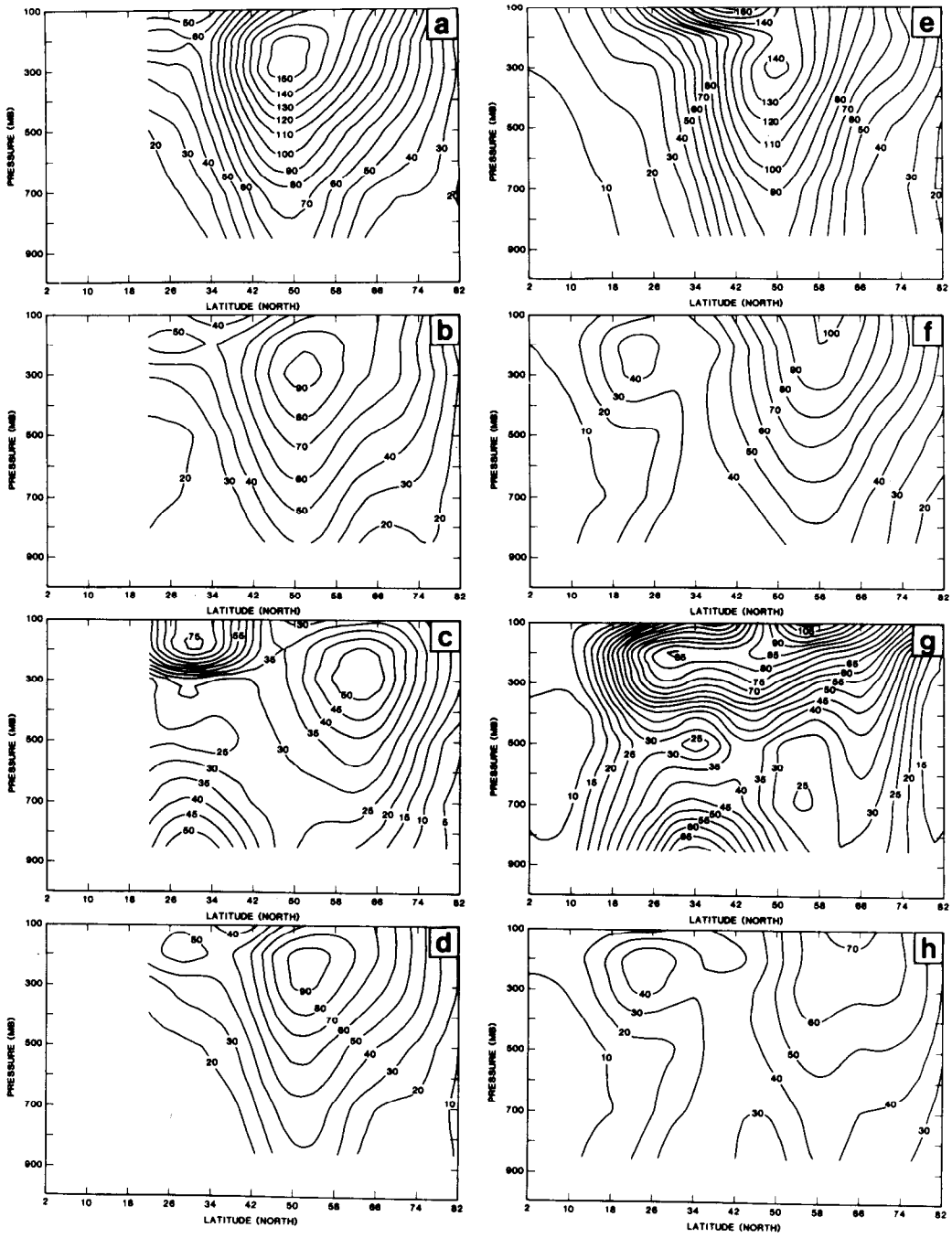

Fig. 5 Latitude-pressure sections of the square root of the zonally averaged stationary eddy variance $([\bar{z}^{*2}])^{1/2}$ for the Northern Hemisphere. (a)–(d) from NMC data: (a) winter (DJF), (b) spring (MAM), (c) summer (JJA) and (d) fall (SON). (e)–(h) from GCM data: (e) winter (DJF), (f) spring (MAM), (g) summer (JJA) and (h) fall (SON). Contour intervals: 5 m for (c) and (g), 10 m for the others.

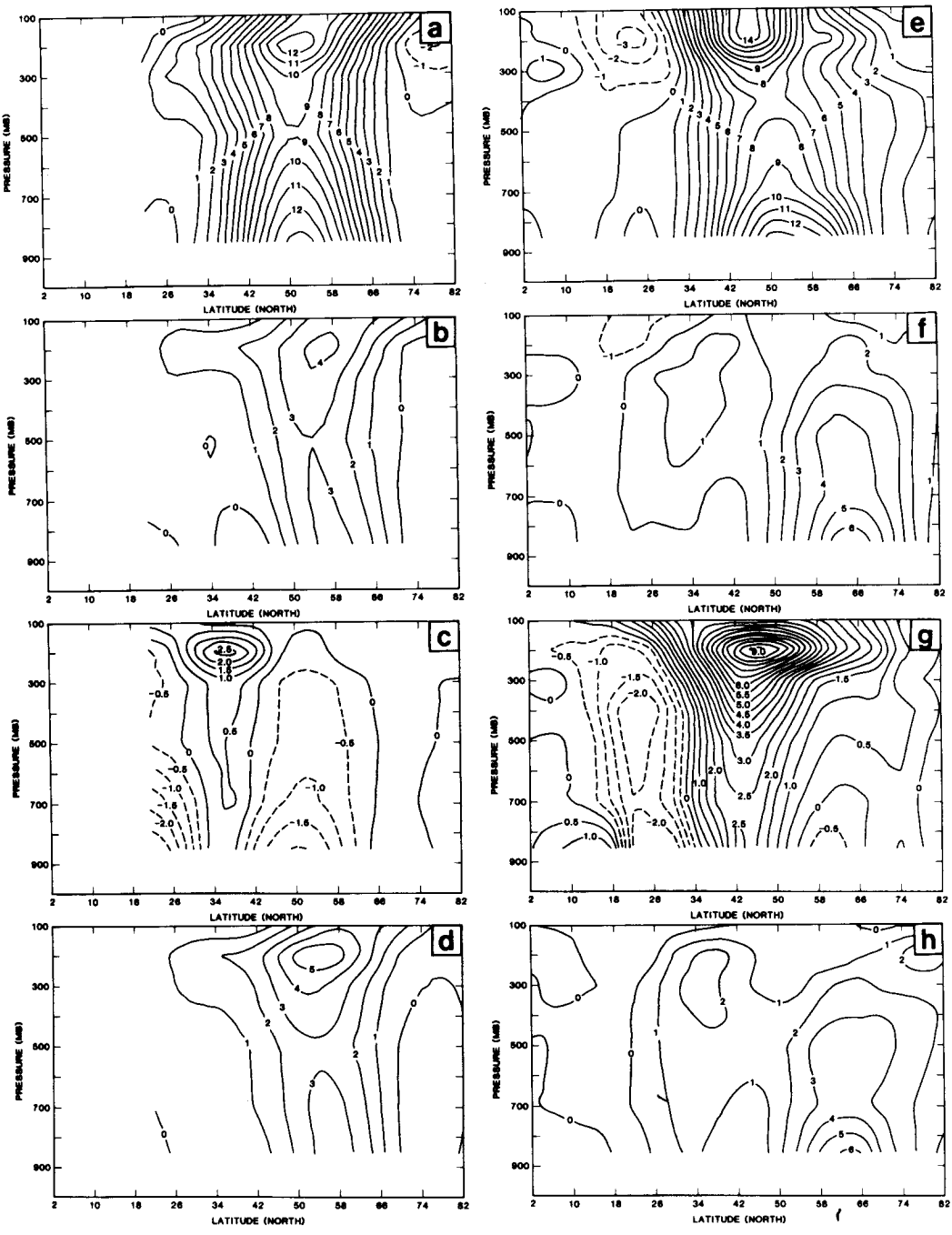

Fig. 6 Latitude-pressure sections of the zonally averaged flux of sensible heat $[\bar{v}^*\bar{T}^*]$ for the Northern Hemisphere. Contour interval: 0.5 m s^{-1} K for (c) and (g); 1.0 m s^{-1} K for all others. Otherwise as in Fig. 5.

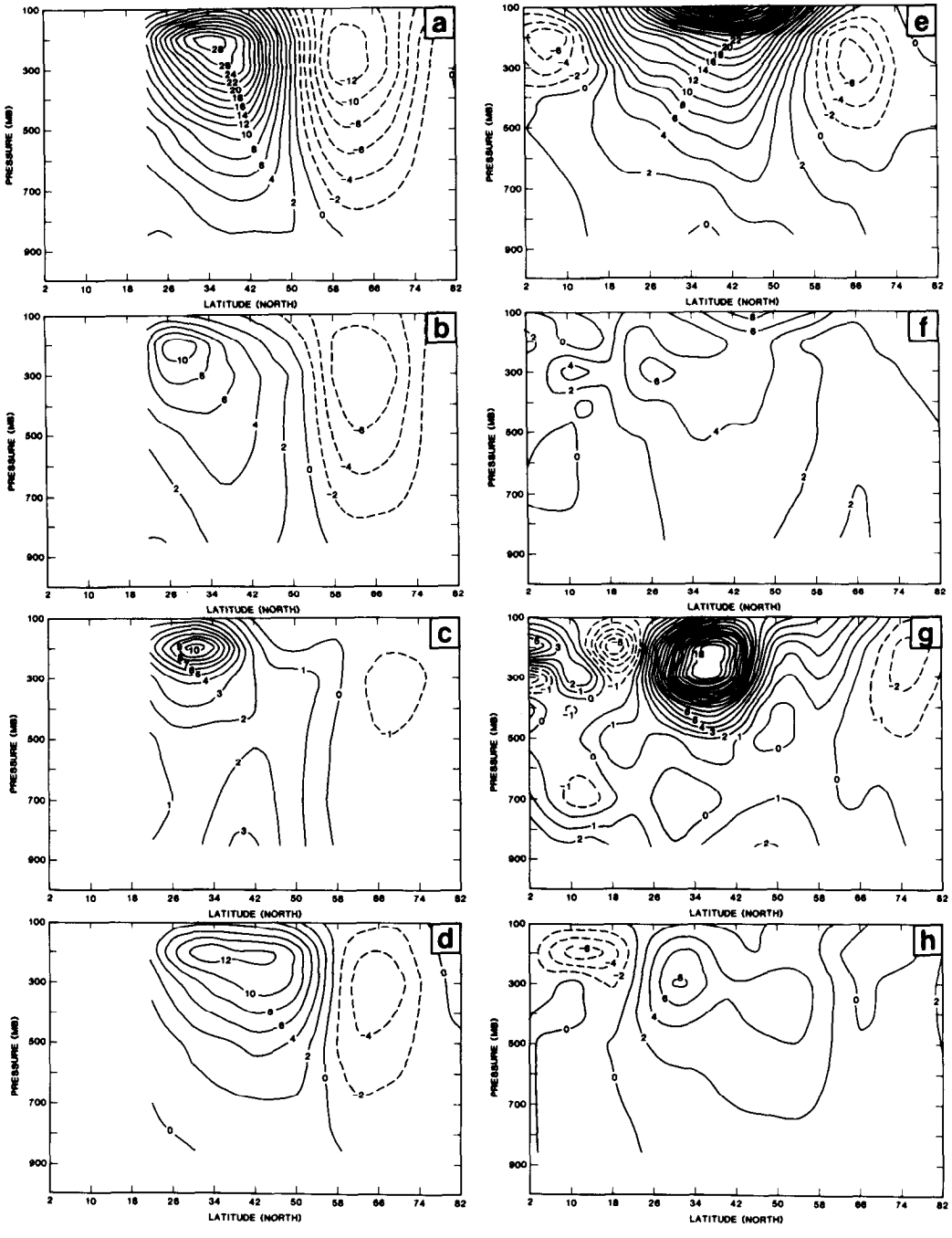

Fig. 7 Latitude-pressure sections of the zonally averaged flux of momentum $[\bar{u}^*\bar{v}^*]$ for the Northern Hemisphere. Contour interval: 1 $m^2 s^{-2}$ for (c) and (g); 2 $m^2 s^{-2}$ for the others. Otherwise as in Fig. 5.

positive centre near 38°N, a negative one near 62°N and a node at about 50°N. This pattern is a result of the well defined tendency for the ridges and troughs of the $\bar{z}^*$ field (see Fig. 1) to tilt from southwest to northeast south of 50°N and to tilt from southeast to northwest polewards of this latitude.

The characteristic dipole pattern is preserved throughout the year, with slight shifts in position and significant changes in amplitude. The maximum (poleward) flux is nearly equal in spring, summer and fall but is much stronger in winter, while the maximum negative (equatorward) flux follows a more regular seasonal cycle, with the least amplitude in summer and the greatest in winter. The position of the zero contour shifts polewards in spring and summer and equatorwards in fall and winter, to some extent mimicking the changes in the position of the mean u-wind $[\bar{u}]$ (see SS1).

The basic dipole structure of the 200-mb winter-time momentum flux is simulated by the GCM such that the centre of the positive (poleward) flux has a realistic magnitude at 200 mb, and the centre of the negative (equatorward) flux is situated too far north, with too small a magnitude (Fig. 7e). This is closely related to the pattern of the GCM's 200-mb $\bar{z}^*$ field in winter (Fig. 2), where the ridges over the high-latitude oceans do not have the correct northwest-to-southeast tilt. The failure of the momentum flux to decrease above 200 mb is typical of many of the GCM's winter eddy statistics, and is presumably closely related to the behaviour of the GCM mean zonal u-wind $[\bar{u}]$ in the winter stratosphere (again see SS1).

The GCM results fail to show the dipole structure in either transition season since the negative centres are absent, a reflection of a poor simulation of the high-latitude eddies. The positive centres are present in the correct locations, although they are too weak. In summer the eddy momentum flux has too large a magnitude (consistent with previously presented summertime results) whereas it has approximately the correct structure, although the negative centre is shifted farther polewards compared with observations.

4 Southern Hemisphere stationary eddies

a *The 500-mb* $\bar{z}^*$

In this section we present the structure of the stationary eddies at 500 mb. Figures 8a–d present the observed stationary eddy field of $\bar{z}^*$ for the four seasons of winter, spring, summer and fall (JJA, SON, DJF and MAM, respectively, in the Southern Hemisphere), along with the GCM results given in Figs 9a–d. (The *total* time-averaged height field is remarkably zonal, so that the troughs (ridges) corresponding to minima (maxima) of the eddy component are hard to see on a plot of total $\bar{z}$ (e.g. see Trenberth, 1979).)

In winter (JJA), the observed eddy height field in the 50–60°S latitude belt is largest polewards of New Zealand, and smallest (most negative) over the Indian Ocean. Around 30–40°S the pattern is nearly the opposite. (The three-month winter mean shown here is in excellent agreement with the July mean $\bar{z}^*$ shown in Trenberth, 1980.)

The transition to spring (SON) is accompanied by a modest overall weakening of the intensity of the eddy field while the pattern remains nearly the same, exhibiting only a slight equatorward shift. The equatorward shift of the overall $\bar{z}^*$ pattern

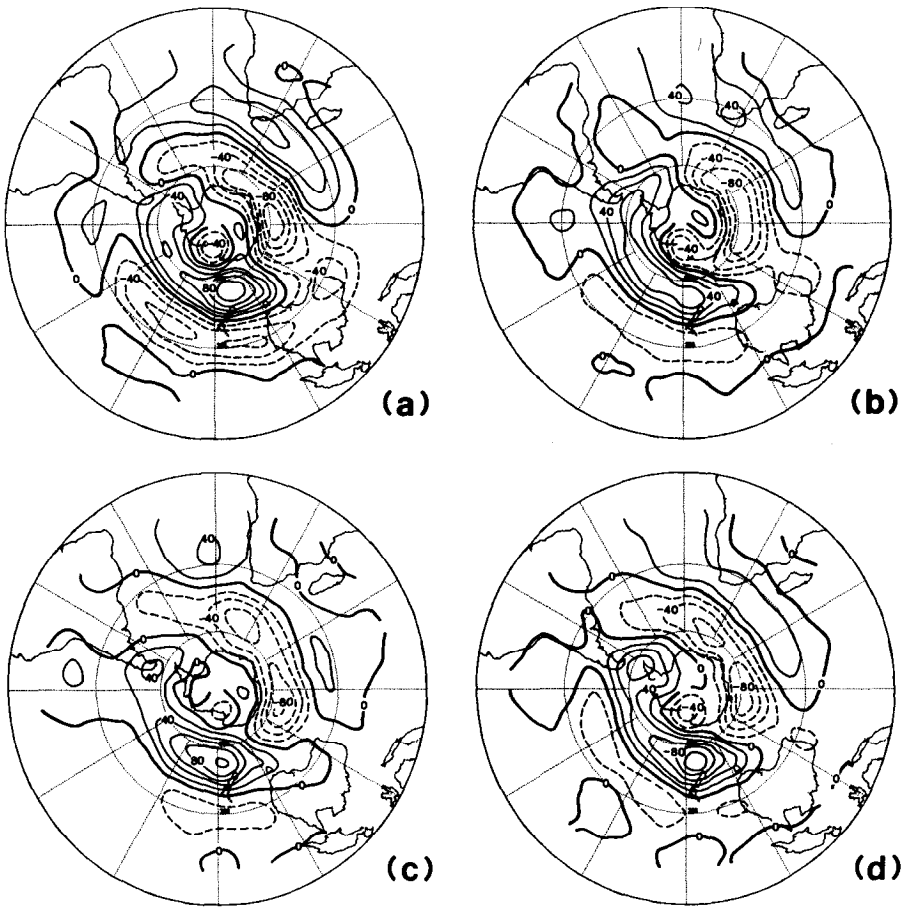

Fig. 8 Stationary eddy component of the 500-mb height field from the Australian data for the Southern Hemisphere: (a) winter (JJA), (b) spring (SON), (c) summer (DJF) and (d) fall (MAM). Contour interval: 20 m.

continues on into the summer (DJF), although the strength of the eddy field remains generally unchanged. Finally, the fall (MAM) pattern represents a movement back towards winter (as in the Northern Hemisphere), with a poleward shift and an overall intensification of the eddies. Although we have emphasized the seasonal changes here, the remarkable degree of uniformity with season so evident in Fig. 8 has been pointed out by many others (see, for example, Trenberth 1979, 1980).

The GCM simulation of the 500-mb $\bar{z}^*$ pattern in winter (Fig. 9a) is unrealistic for geographical locations in high latitudes, although the overall magnitudes are reasonable. In the subtropics (where the simulation is better), the maximum off South Africa is too weak while the minimum off the coast of Australia is not extensive enough.

M present the total winter mean 300-mb geopotential height field in the Southern Hemisphere in their Fig. 8. It is apparent that the eddy field is too weak in most locations.

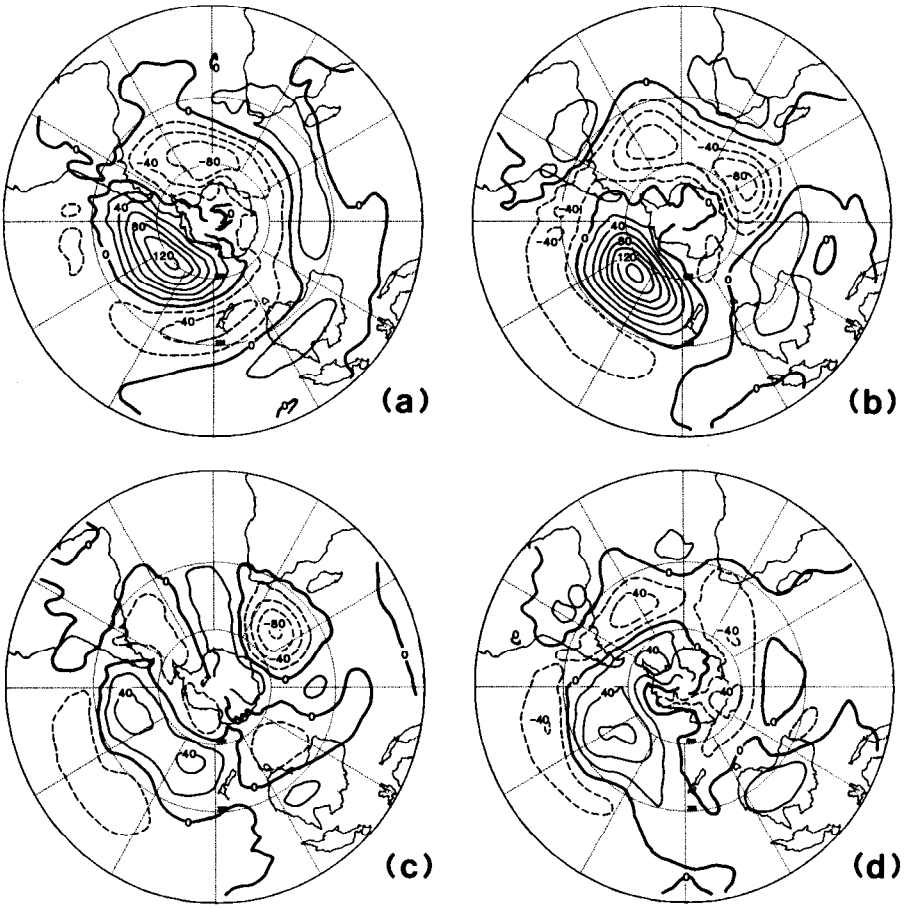

Fig. 9 As in Fig. 8, except for the GCM data.

In spring (SON), the simulation is more realistic. However, the observed high-latitude Pacific maximum is far too intense (although situated fairly realistically) while the Indian Ocean minimum extends too far westwards, as in winter.

The weakening of the simulated eddy field in passing from spring to summer (DJF) is excessive. Nevertheless, the pattern is now realistic in mid-latitudes, except for an anomalous (weak) maximum in the Pacific. A corresponding summer map for the CCM is not shown in M, but the authors mention that the stationary waves are "... quite deficient ...", being far too weak.

The GCM eddy pattern in the southern Fall (MAM) is similar to the simulated pattern in winter. The Pacific maximum is 60° too far east (as in winter) but is now too weak, while the large-scale Indian Ocean minimum again extends too far west and is weak.

The overall degree of uniformity with season seen in the observations is present only to some extent in the GCM results. The Pacific sector correctly shows consistent-

ly positive values of $\bar{z}^*$ and the Indian Ocean sector consistently negative ones. The extreme seasonal range of the magnitude in the Pacific (120 m in winter compared to 40 m in summer) and the variability of the subtropical eddy field over the Indian Ocean are unrealistic, however.

b *Vertical Structure of Variances and Covariances*

To portray the vertical structure of the stationary waves in the Southern Hemisphere, we use results based on the ECMWF analysis of the GWE year, because the data coverage in the Southern Hemisphere was reasonably good. By using data from one year only we are ignoring the interannual variability of the atmosphere, a problem made worse by the somewhat unusual behaviour of the Southern Hemisphere during the GWE year (Trenberth, 1984). The results of this section must be interpreted with this caution in mind. As a check on the ECMWF results, we will compare them with the GFDL analyses of the same year, as reported in Lau (1984).

Latitude-height sections of the observed (ECMWF) rms of the stationary eddy height field $[\bar{z}^{*2}]^{1/2}$ are presented in Figs 10a–d.

The winter eddy rms height field reaches a peak of 60 m at 150 mb in the subtropics, and increases up to 100 mb at 60°S, reaching a value of 125 m there. Note that at the 200-mb level the Southern Hemisphere stationary rms is weaker than its Northern Hemisphere counterpart (compare Figs 5a and 10a), but that the reverse is true at 100 mb. The presence of two maxima in the rms eddy field is clearly related to the double maximum in the mean flow $[\bar{u}]$ (see SS1).

As indicated by the 500-mb $\bar{z}^*$ maps, the transition to spring is accompanied by only a rather subtle change in the stationary eddy pattern, with virtually no change in high latitudes and a modest weakening and equatorward shift in the subtropics. The passage into summer leads to more distinctive changes, with both peaks weakening and moving towards the equator. The rms at 55°S now peaks in the troposphere, indicative of the trapping of the stationary waves by the stratospheric easterlies. A movement towards winter conditions is indicated in the transition from summer to fall, with the strengthening and poleward shifts of both peaks (particularly the subtropical one), and the increased penetration of stationary waves into the stratosphere at high latitudes. The double-jet structure in $[\bar{u}]$, which disappears in summer, begins to re-establish itself in fall. The behaviour of the stationary eddy height rms depicted here from the ECMWF analyses is in substantial agreement with the corresponding GFDL results.

Turning to the GCM results, we see that in winter the model correctly predicts a high-latitude maximum and a subtropical one. At 200 mb the high-latitude maximum is about 20% too weak and fails to increase above this level, indicating less stratospheric penetration than that observed. Below 250 mb the structure of the simulated results is quite good in mid-latitudes. The subtropical maximum, however, is weaker than in the GWE analyses and is located too far equatorwards. This is probably related to the nature of the simulated $[\bar{u}]$ field, which does not show the double-jet structure observed during the GWE year.

The Southern Hemisphere winter rms of stationary eddies for the CCM is quite similar to the GLAS results (Fig. 10e) below about 200 mb, but the CCM captures better the observed stratospheric penetration. Note that the GLAS GCM's rms in the

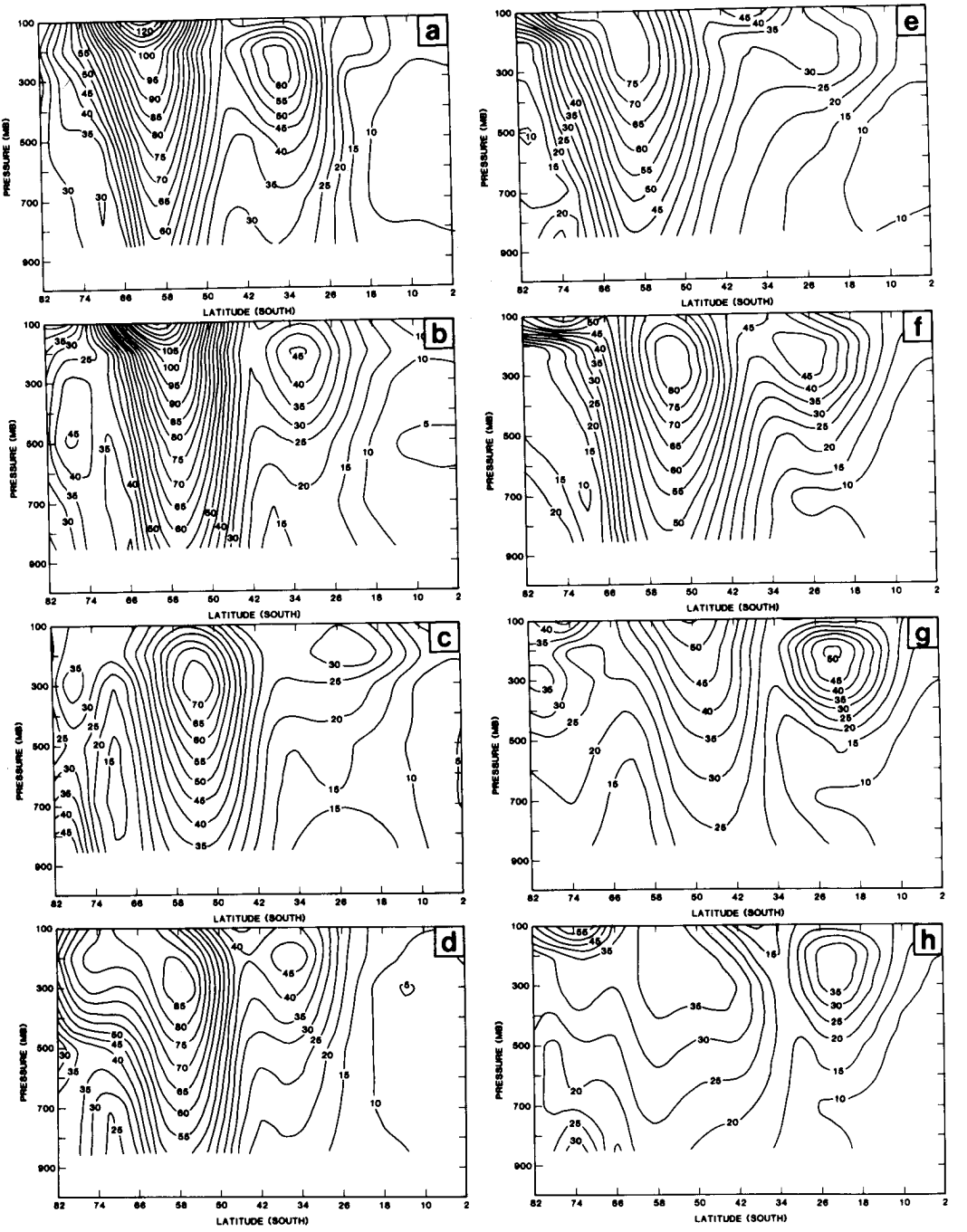

Fig. 10 Latitude-pressure sections of the square root of the zonally averaged stationary eddy variance $([\bar{z}^{*2}])^{1/2}$ for the Southern Hemisphere; (a)–(d) from the ECMWF GWE data: (a) winter (JJA), (b) spring (SON), (c) summer (DJF) and (d) fall (MAM). (e)–(h) are the corresponding fields for the GCM data. Contour interval: 5 m.

subtropics agrees quite well with the *observations* reported in M, which they obtained from van Loon and Jenne (1972) and van Loon et al. (1973).

The mid-latitude maximum remains nearly constant in magnitude in the winter-to-spring transition, and continues to show too little stratospheric penetration. The distinct equatorward shift of this feature is realistic, however. The subtropical maximum is realistic.

In the southern summer, the GCM's rms is somewhat weak, and exhibits too much stratospheric penetration. The simulated subtropical maximum is much stronger than observed. The corresponding CCM results for the southern summer indicate an extremely weak rms everywhere, considerably less intense than in the GLAS GCM results. Although there is some evidence of a movement towards winter conditions in the GCM's fall results, (e.g. the poleward shift of the mid-latitude maximum), the progression of summer-to-winter states is much less smooth than in nature. The mid-latitude maximum itself is far too weak at 200 mb near 50°S, but the values at 100 mb at high latitudes are not unrealistic.

Some of the deficiencies of the simulated stationary eddy rms (such as the excessive stratospheric penetration in the southern summer) are clearly related to the errors in the model's basic state described in SS1 (where the GCM's subtropical jet does not close at upper levels in DJF). Whether all the errors in the simulation can be explained in this manner is not possible to determine without the use of a compatible stationary wave model.

In an overall sense, the stationary eddies are most realistic below 200 mb in both winter and spring.

5 Transient fluctuations in the Northern Hemisphere

Transient fluctuations are defined here as those fluctuations that remain after the annual mean, annual harmonic and semi-annual harmonic have all been removed (see SS1). In some cases the data have been time-filtered in order to isolate growing baroclinic disturbances from the low-frequency background. The so called "band-pass" filter retains periods of about 2 to 10 d, and was suggested by Blackmon and White (1982). It is a somewhat broader filter than the more conventional filter first used by Blackmon (1976) that retains only periods of about 2 to 6 d. The impetus for extending the filter came from the work of Simmons and Hoskins (1978) on the life cycle of baroclinically unstable waves. They found that waves of zonal wavenumber 6 have periods close to the low-frequency end of the Blackmon (1976) filter, and therefore might be partially truncated by it.

Maps of the square root of the total 500-mb geopotential height variance (not shown) indicate that in winter, maxima occur over the eastern Pacific and Atlantic oceans, regions associated with ridges in the time mean height field (Blackmon, 1976, hereafter referred to as B76). A band of high rms also extends eastward over northern Europe and Russia. The pattern for spring looks nearly identical with that for winter, both in terms of overall magnitude and geographical distribution. Summer is marked by a considerable weakening of the Pacific maximum (although without much of a shift in position) and a decline in the rms strength over the Atlantic in comparison with the rms values over Scandinavia and northern Russia. The rms distribution in fall is very similar to that in winter.

The simulated maps of 500-mb rms height (not shown) indicate that the GCM is fairly successful in capturing the geographic pattern of variability in all seasons but summer, when the Atlantic maximum is not simulated and the Pacific maximum is displaced somewhat to the north.

The success of the GLAS GCM is not shared by the NCAR CCM. As shown in Fig. 14a of M, the CCM predicts very intense, spurious maxima in rms over Alaska and Greenland in winter, leading to a very unrealistic pattern. In summer the pattern simulated by the CCM is weak and nearly featureless.

A discussion of the overall magnitudes of the zonally averaged variance is given below in conjunction with Figs 13 and 14.

Maps of the (co)variances of fields that have been prefiltered with a band-pass filter emphasize the regions of developing baroclinic disturbances, effectively focusing on the major oceanic "storm tracks" (B76; Blackmon et al., 1977). A good example of this is Fig. 11a, which shows the NMC winter map of 500-mb rms height, in which the height field has been first filtered with the band-pass filter discussed above. (In addition the height field was spatially filtered to remove zonal wavenumbers higher than 20.) A broad maximum is seen over Newfoundland, extending east-northeast into the Atlantic, and a somewhat broader maximum originates off the east coast of Asia and extends east-northeast over much of the Pacific. The behaviour of a number of other diagnostics confirms that these are the regions characterized by active baroclinic development. For example, the very broad extent of the Pacific storm track is seen in the map of the winter-time correlation coefficient between the 500- and 1000-mb band-pass heights presented in Blackmon et al., (1979). They find that the correlation is fairly low (~0.5) over most of the Pacific, and increases only near the western coast of North America, reflecting the predominance of the more barotropic decay phase of the storms there. Similar results were found by Lau (1979a), who used cross-spectrum analysis to examine the phase lag of 500-mb height relative to 850-mb height in the 4.5–6 d range, and found that while this phase lag decreases across the Pacific, it remains fairly constant from the western edge of the storm track to the date-line, and only changes noticeably near the west coast of North America. Maps of the transient variance of vertical velocity and of the covariance between vertical velocity and temperature shown by Lau (1979a) indicate broad agreement with Fig. 11a regarding locations of the storm tracks.

The positions of the "storm tracks" are remarkably consistent from season to season (Figs. 11a–d), shifting only slightly poleward (from their winter-time positions) in the transition seasons and more noticeably in summer. The summer's filtered rms is weaker than that of the other seasons, which are equally vigorous.

The GLAS GCM is very successful in simulating the positions and intensities of the maxima in band-pass rms in all seasons but summer, as shown in Figs 12a–d. Even in summer the overall magnitudes are realistic, but the pattern is somewhat distorted. The winter map of band-pass height rms for the CCM, given in Fig. 15 of M, is also quite realistic. However, the summer rms (Fig. 29 of M) is excessively weak.

We have examined maps of the Northern Hemisphere transient heat flux $\overline{v'T'}$ at 850 mb and of the band-pass transient momentum flux $\overline{u'v'}$ at 200 mb in order to determine the seasonal dependence of the geographic patterns. The heat flux peaks over the oceanic storm tracks, with the Atlantic maximum extending westwards, well inland

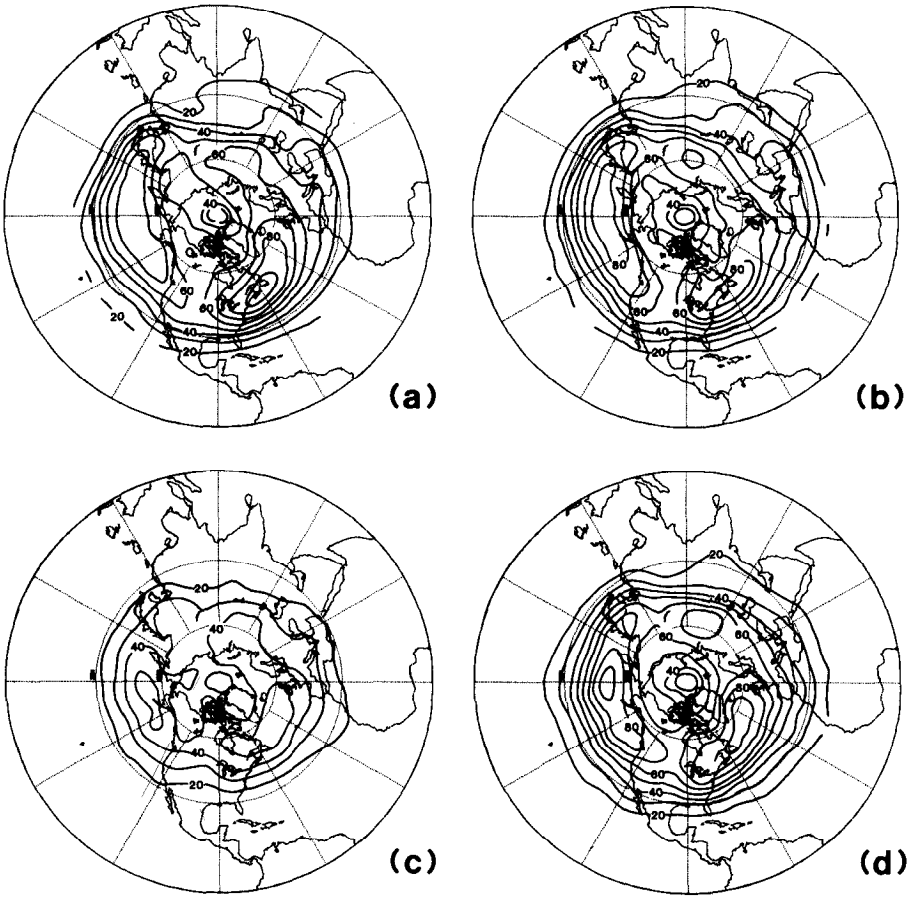

Fig. 11 Transient rms of the 500-mb band-pass height for the Northern Hemisphere from NMC data: (a) winter (DJF), (b) spring (MAM), (c) summer (JJA) and (d) fall (SON). Contour interval: 10 m.

over North America. A peak is seen in the Gulf of Alaska only during winter, but otherwise the seasonal dependence is very similar to that of the band-pass height. The geographic structure of the transient heat flux in the GLAS GCM (not shown) is quite realistic in all seasons but summer, when again the overall magnitudes of the flux are realistic but the well defined maxima that have been observed do not appear.

The 200-mb band-pass momentum flux (not shown) shows maximum convergence over the oceanic storm tracks, with a maximum flux to the south, and a (weaker) maximum equatorward flux to the north. An additional peak over the West Coast of North America appears in all seasons but summer. The simulated pattern is fairly realistic in winter and spring, but again is too featureless in summer, whereas the observed Pacific maximum in convergence is missing in fall. The strength of the equatorward flux centres is generally too weak in the GCM results, and the maximum over western North America is not simulated in any season.

The overall magnitude of the transient variances and fluxes are summarized in Figs.

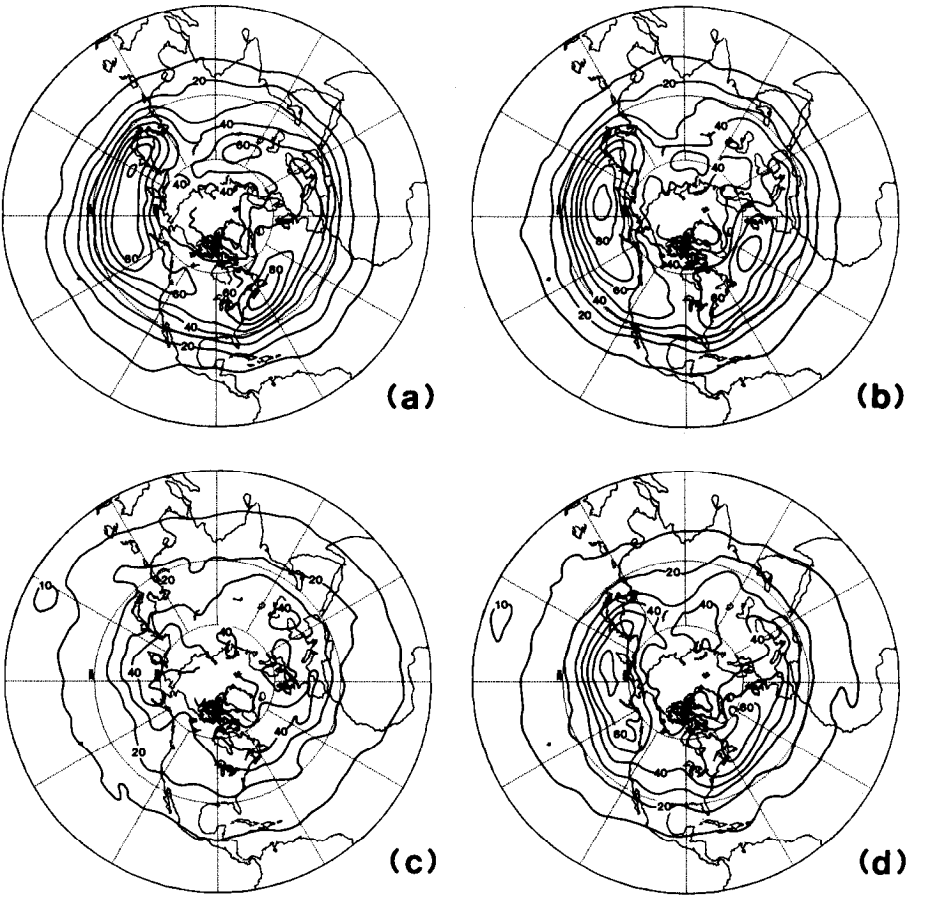

Fig. 12 As Fig. 11, except for the GCM data.

13 and 14, which show latitude-height sections of the zonally averaged heat and momentum fluxes and the square root of the zonally averaged height variance, all calculated from the ECMWF-7 analyses and from the GCM for both winter and summer. The winter simulation of the transient height variance (Figs 13a and d) is quite realistic. Although the GCM rms is slightly too weak, the latitude-height structure is well captured. The transient momentum flux is extremely well simulated, the only major difference between the model results and the ECMWF-7 analyses being the absence in the GCM of the distinct negative centre observed at 200 mb in high latitudes.

The low-level heat flux is also quite realistic in the GCM, but the model heat flux increases above 850 mb (rather than decreasing, as the ECMWF-7 analyses show) and reaches a peak at 500 mb. An interesting result in the simulation at 200 mb is the equatorward heat flux at high latitudes, which contributes to a distinct maximum in heat flux convergence at 50°N at upper levels. To determine whether this feature

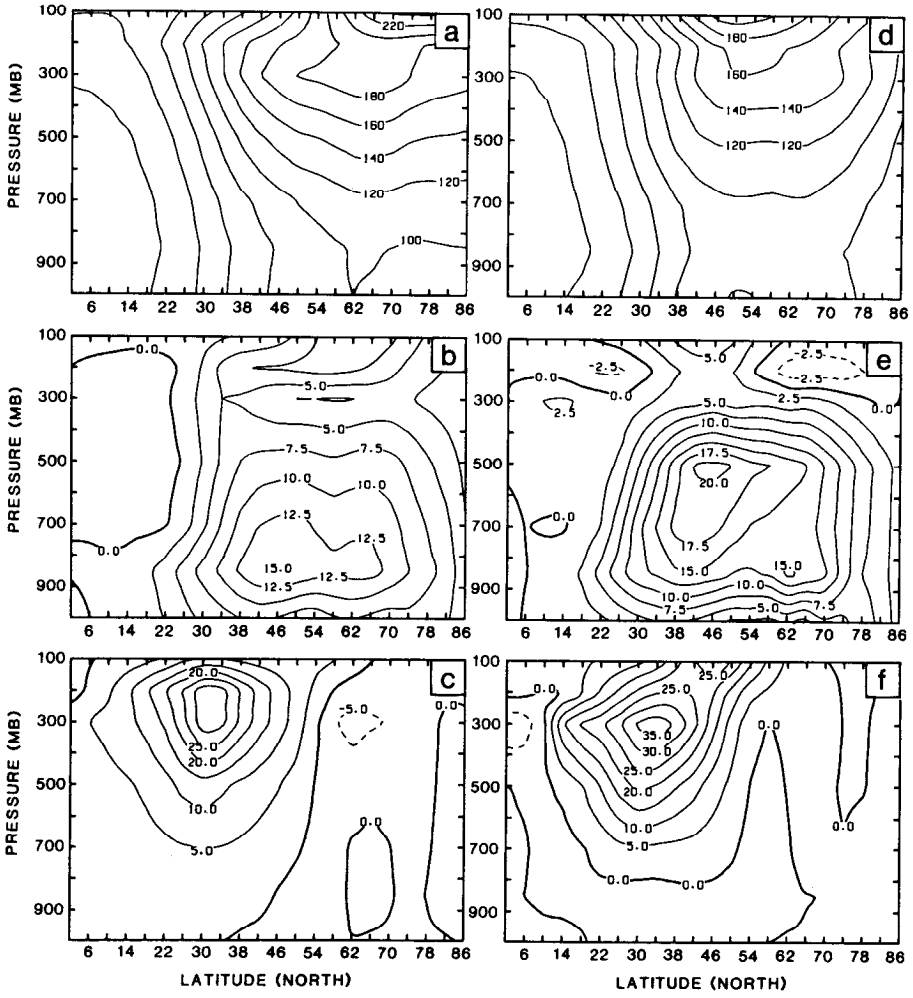

Fig. 13 Latitude-height sections of (a) the square root of the zonally averaged transient height variance (contour interval: 20 m), (b) the zonally averaged transient heat flux (contour interval: 2.5 m s^{-1} K) and (c) the zonally averaged transient momentum flux (contour interval: 5 m^2 s^{-2}), all from the 7-year set of ECMWF analyses for the northern winter (DJF). (d)–(f) are the corresponding fields for the GCM.

contributes significantly to the excess cooling at the pole would require a study of the upper-level sensible heat budget. (Note that this feature is not present in summer.)

In summer (Fig. 14) the GCM's transient height rms is quite realistic below 150 mb, the level of the observed maximum. However, the GCM eddies are too active at 100 mb, where the ECMWF-7 analyses show a distinct decrease in rms. As in winter, the transient heat flux is realistically simulated at lower levels, but again shows a large spurious peak at 500 mb. The transient momentum flux simulation is unrealistic.

The question of compensation between transient and stationary fluxes is an interest-

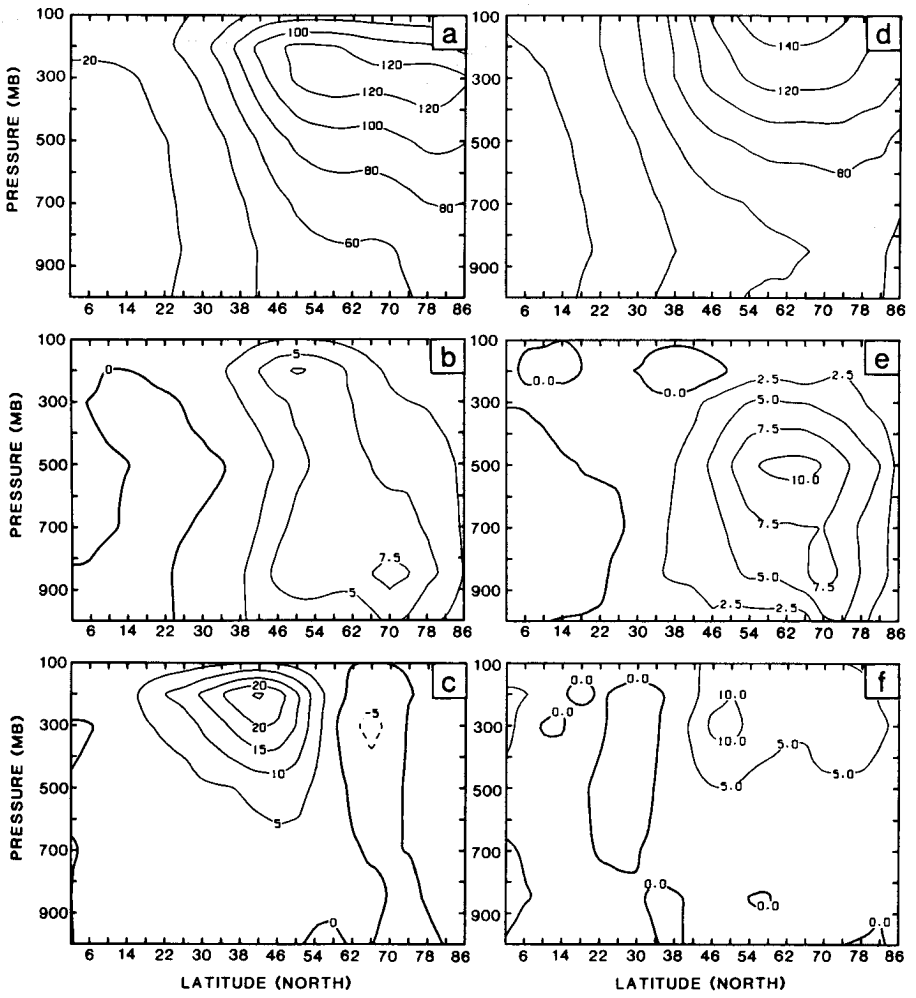

Fig. 14 As Fig. 13, except for the northern summer (JJA).

ing one. By comparing Figs 5–7 with Figs 13–14, we notice that such a compensation does take place in certain cases, but it is not pervasive. For example, the slight weakness of the simulated winter stationary eddy heat flux at mid-levels is (over)compensated by a stronger model transient flux. Also, the overly strong stationary eddy momentum flux simulated at upper levels in summer is compensated by an overly weak simulation of the transient momentum flux. A counter example is the simulation of the summertime eddy heat flux at mid-levels, for which both the stationary and transient components are too strong. (Note, however, that since the transient components are taken as deviations about the seasonal cycle (and not the seasonal mean), the total variance of any quantity (or the total flux) will not be just the sum of the stationary and transient components, but will involve other terms (Straus, 1983). In this context these terms are expected to be small.)

6 Transient fluctuations in the Southern Hemisphere

a *The 500-mb Geopotential Height*

The square root of the total transient 500-mb height variance $(\overline{z'^2})^{1/2}$ for the southern winter (JJA), as obtained from the Australian data set, has three distinct maxima (Fig. 15a). One is poleward of New Zealand, one southeast of South America, and one in the Indian Ocean. As pointed out by Trenberth (1982), the latter is associated with the major storm track in the Southern Hemisphere, whereas the other two are associated with lower frequency fluctuations. Our winter (JJA) and summer (DJF) results for total rms agree fairly well with those of Trenberth (1982), who used 128-d seasons. However, there are some differences in magnitude (but not in pattern) when it comes to the band-pass results to be discussed below, for Trenberth used quite different time filters.

There is little change from winter conditions in the spring pattern (not shown), whereas summer is accompanied by an equatorward shift of the maximum south of New Zealand and a weakening of the rms in the Indian Ocean (Fig. 15b). In fall, the total rms again looks very similar to that of winter, and is therefore not shown.

While the GCM winter rms is generally too vigorous (Fig. 15c), the basic pattern is realistic with the exception of a spurious maximum at high latitudes in the Pacific and a distinct eastward displacement of the maximum in the New Zealand sector. Interestingly, the CCM shows a similar high-latitude Pacific anomaly in the JJA 500-mb rms height, as shown in Fig. 22 of M.

The GCM's simulation of the transition to spring (not shown) is realistic in the Indian Ocean, where the winter maximum remains nearly unchanged, but it is not good in the Atlantic (where the observed centre off South America is not present), nor in the Pacific, where the spurious maximum broadens, almost engulfing the centre poleward of New Zealand. The GCM rms for summer (DJF) is fairly realistic (Fig. 15d), although the simulated peak in the Pacific and the variability in the Atlantic are too strong. (The Pacific anomaly is seen once again in the southern summer results of the CCM (Fig. 32 of M). However, the CCM is generally too quiescent.) In the GCM fall results (not shown), the spurious Pacific centre remains, while the observed maximum off South America is absent (although the rms is high there) and the New Zealand maximum is shifted 45° to the west.

The low-pass filtered rms for winter from the Australian data (not shown) is quite similar to that presented by Trenberth (1982), with maxima in locations similar to the total rms locations. The band-pass filtered winter rms (shown in Fig. 16a) identifies a broad storm track in the Indian Ocean. (The values of the rms in our Fig. 16a are a factor of two less than those in Fig. 11a of Trenberth (1982). This is primarily due to the very different filters used.) In the Pacific, the rms is weaker, but a maximum in the meridional profile does exist.

The Indian Ocean storm track and the weak maximum in the Pacific profile are virtually unchanged in spring (not shown). In summer (Fig. 16b) the only change is a very slight weakening of the storm tracks. The band-pass rms in fall is nearly identical with that in spring.

The simulation of the winter band-pass rms in both the GLAS GCM (Fig. 16b) and

the CCM (Fig. 23 of M) are quite realistic in terms of the location of the main storm tracks, but the GLAS GCM is much too vigorous in this frequency range. The CCM in contrast, is too quiet. The GLAS GCM simulated band-pass rms remains nearly unchanged in spring (not shown), although a small poleward shift is discernible in the peak values in the Pacific. In summertime the main (Indian Ocean) storm track weakens slightly but does not move (Fig. 16d), in good agreement with the observations. Again the magnitude of the rms is excessive in the GLAS simulation. (The CCM also shows realistic storm tracks in the southern summer, but the rms is once again too low.) The simulated storm track in fall is very similar to that in spring over the Indian Ocean, but is somewhat stronger in the Atlantic and Pacific oceans, so that the fall band-pass rms pattern is one of a nearly continuous circumpolar storm track.

The overall transient eddy (co)variance is indicated in Figs 17 and 18, which compare latitude-height sections of the square root of the zonally averaged transient height variance and the zonally averaged heat and momentum fluxes for the solstitial seasons from the GCM with those from the ECMWF-7 analyses. The GCM simulates the overall transient eddy activity quite well, especially in winter. However, the GCM height rms fails to decrease in the lower stratosphere as is observed in summer, a result we have already noted for the stationary wave height rms. In addition, the transient (poleward) heat flux is too large at mid-levels, as it is in the Northern Hemisphere. The momentum flux is well simulated in both seasons, with the exception of the summertime branch of the equatorward flux occurring at high latitudes and at 200 mb, which is too weak in the GCM.

7 Discussion

Some of the errors in the simulation of stationary and transient fluctuations by the GLAS GCM can be understood qualitatively in terms of the linear (and non-linear) responses to anomalies in heating. In addition, inaccuracies in the simulated (two-dimensional) basic state are clearly important. In the absence of careful experiments with compatible linear models, these interpretations cannot be made rigorous. However, certain conclusions seem warranted on the basis of the evidence presented.

The stationary eddies in the Northern Hemisphere below about 300 mb are more accurately captured by the GLAS GCM in the winter season than in the summer season. This is also true to some extent for the CCM, although the latitude-height structure of the summer stationary variance is well simulated by this model; it is only the geographical pattern in the northern summer that is not completely realistic. At upper levels the CCM's stationary waves are more realistic than those of the GLAS GCM, a result that is most likely due to the superior simulation of the upper-level zonal winds by the CCM.

A strong candidate for the forcing that causes this seasonal dependence of stationary wave errors in the Northern Hemisphere is that due to latent heat release. The precipitation is more poorly simulated in the northern summer than in the northern winter, the nature of the summertime errors in the GLAS GCM consisting of excessive continental rainfall in general as well as anomalous rainfall over the Sahara (see SS1). (The CCM also predicts too much rainfall over North America in summer.)

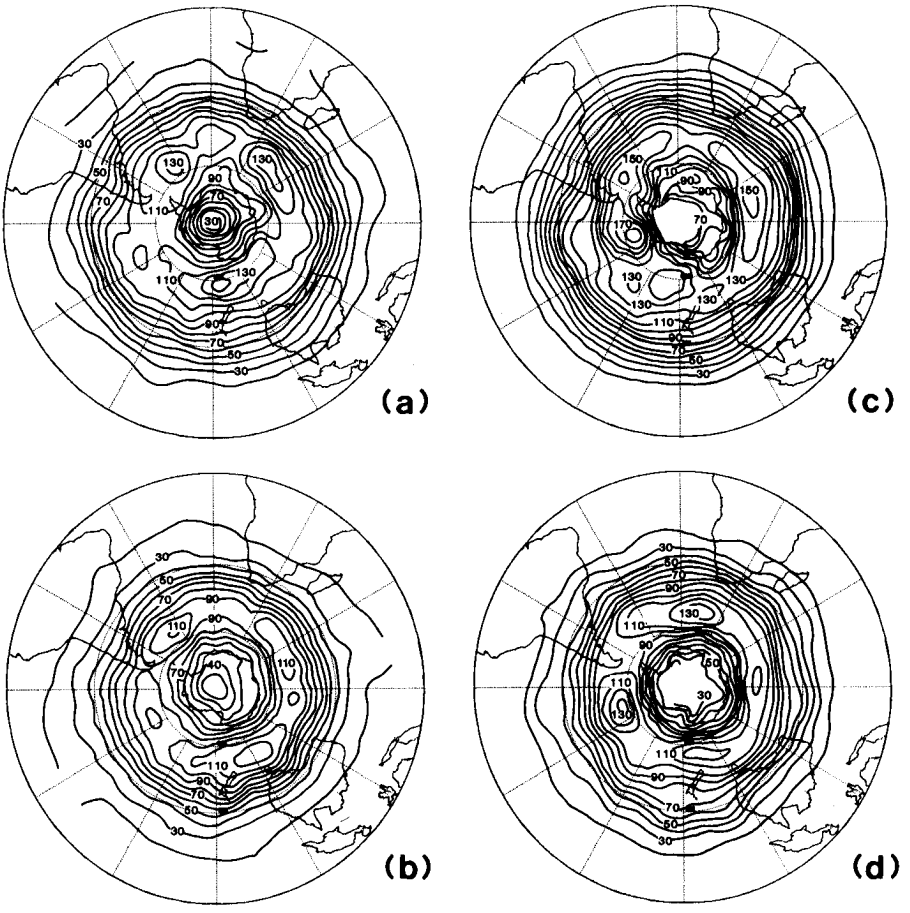

Fig. 15 Square root of the transient 500-mb height variance for the Southern Hemisphere; (a) southern winter (JJA) from the Australian data, (b) southern summer (DJF) from the Australian data, (c) southern winter (JJA) from the GCM, and (d) southern summer (DJF) from the GCM. Contour interval: 10 m.

Whether heating anomalies in the tropics or in mid-latitudes are primarily responsible for the stationary wave anomalies is hard to say, for the responses to these two forcings may interfere constructively or destructively (Lindzen et al., 1982).

The superiority of the simulation in the northern winter to that in the northern summer is seen in the GLAS GCM transient eddy statistics also, in particular, in the geographic distribution of both the total and band-pass rms of 500-mb height, and in the zonally averaged momentum flux. (For the CCM, the seasonal dependence is seen more clearly in the band-pass rms, for the Northern Hemisphere total transient rms is not very realistic in either season.) It is not immediately clear how this seasonal dependence is related to either tropical or mid-latitude precipitation in the northern summer, but it is clear that significant stationary wave errors should strongly influence the transient fluctuations.

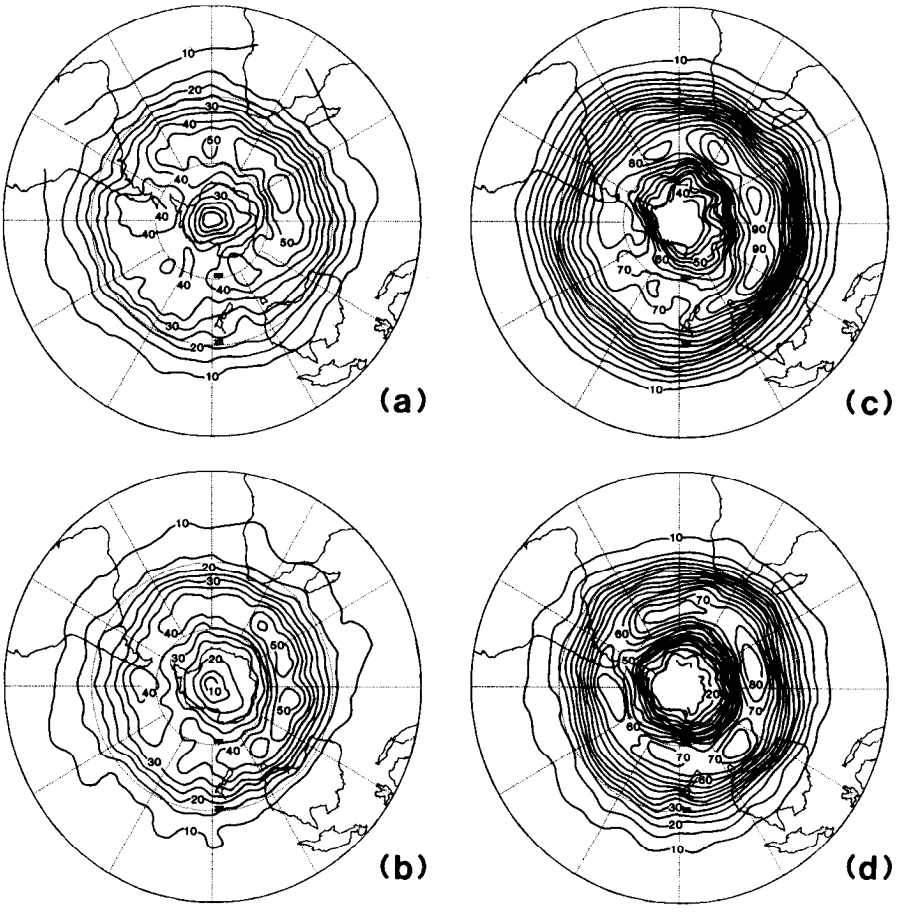

Fig. 16 As Fig. 15, except for the square root of the band-pass 500-mb height variance; contour interval: 5 m.

A seasonal dependence in the stationary waves simulated by the GLAS GCM is also seen in the Southern Hemisphere, although it is not as obvious as in the Northern Hemisphere; below 200 mb, the stationary wave rms appears more realistic in winter and spring than in summer and fall (Fig. 10). (In the CCM, the seasonal dependence is stronger, with the stationary waves being much too weak in the southern summer.) As discussed in SS1, the DJF precipitation averaged between the equator and 20°S is excessive in both GCMs, so that we should expect some problems with the simulated stationary waves in the Southern Hemisphere. (An example of Southern Hemisphere sensitivity to tropical latent heat release is given by Kalnay et al., 1986). Note that the excessive quietness of the CCM in the Southern Hemisphere does not necessarily rule out this explanation: The linear responses to mountains and heating can interfere destructively, so that an increase in one component of the forcing need not lead to an increase in the amplitude of the response everywhere.

An overall feature of the GLAS GCM is its generally superior skill in simulating the

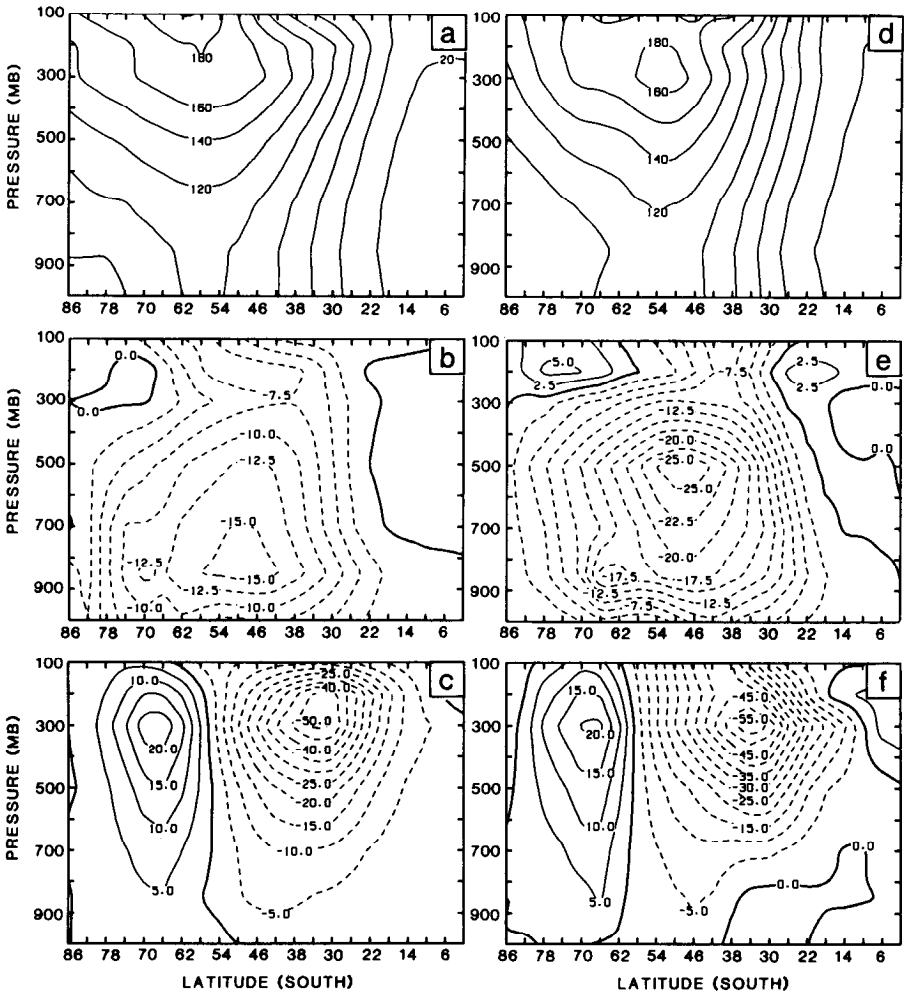

Fig. 17 As Fig. 13, except for the southern winter (JJA).

stationary eddies of the Northern Hemisphere compared with those of the Southern Hemisphere. Asymmetries in the Southern Hemisphere are forced by the large difference between Atlantic and Pacific sea surface temperatures present throughout the year in mid-latitudes (van Loon, 1972a, b; van Loon and Jenne, 1972), by the asymmetry of the Antarctic continent (van Loon, 1972a, b), by the Antarctic topography (Grose and Hoskins, 1979) and by topography in general in the Southern Hemisphere (Mechoso, 1981; Jarraud et al., 1986). The latter papers emphasize that the transient flow as well as the stationary flow is strongly affected by the mountains in the Southern Hemisphere (viz. the Andes, the African plateau, and the massive ice dome of East Antarctica). Since these forcings are taken into account in the GCM, it is not clear why the simulation of stationary waves is poorer in the Southern Hemisphere.

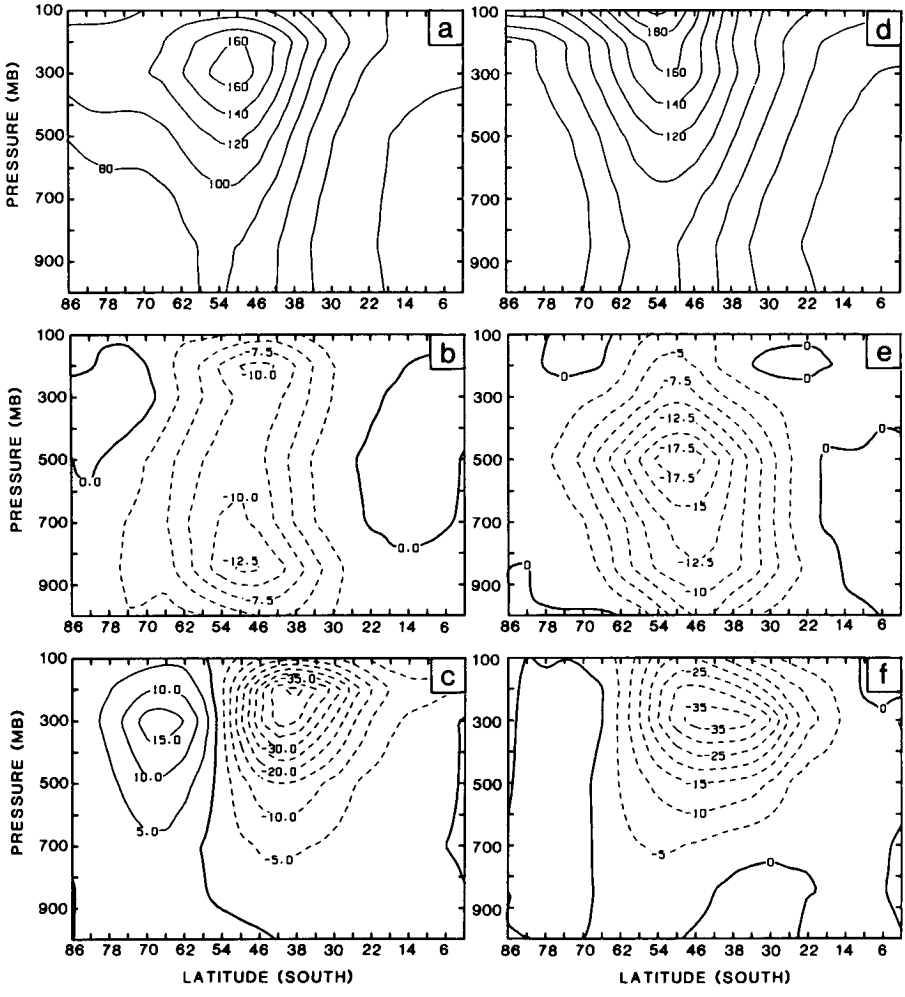

Fig. 18 As Fig. 17, except for the southern summer (DJF).

It is interesting to note that an overall hemispheric difference in the skill of the GLAS GCM simulation of the transient waves is not apparent from Figs 13–14 and 17–18, in distinct contrast to the CCM. Indeed, the winter-time simulation of the zonally averaged transient height rms and momentum flux in both hemispheres is quite successful. As discussed in SS1, Palmer et al. (1986) argue that low-resolution GCMs tend to substantially underestimate the atmospheric momentum flux convergence. It is clear from this paper (and from the vertically integrated convergence of total momentum flux presented in SS1) that, although inaccuracies in the individual components of the momentum flux appear in the simulation (especially in summer), the total flux is fairly well simulated by the GLAS GCM. In at least some respects, then, the GLAS GCM results are typical of an intermediate resolution model.

In order to achieve a greater understanding of the comparative strengths and

weaknesses of models with varying resolutions and physical parametrizations, we hope to extend this type of analysis to annual cycle integrations of other GCMs in the future.

Acknowledgements

We owe special thanks to many people for their help and encouragement in completing this project: M. Halem, E. Kalnay, L. Marx, Y. Mintz, D. Randall and Y. Sud. The programming support of J. Ardizzone and the drafting work of L. Rumburg are also greatly appreciated. The comments of the anonymous referees are appreciated.

References

BLACKMON, M.L. 1976. A climatological spectral study of the 500 mb geopotential height of the Northern Hemisphere. *J. Atmos. Sci.* **33**: 1607–1623.

——— and G.H. WHITE. 1982. Zonal wavenumber characteristics of Northern Hemisphere transient eddies. *J. Atmos. Sci.* **39**: 1985–1998.

———; J.M. WALLACE, N.-C. LAU and S. L. MULLEN. 1977. An observational study of the Northern Hemisphere wintertime circulation. *J. Atmos. Sci.* **34**: 1040–1053.

———; R.A. MADDEN, J.M. WALLACE and D.S. GUTZLER. 1979. Geographical variations in the vertical structure of geopotential height fluctuations. *J. Atmos. Sci.* **36**: 2450–2466.

GROSE, W.L. and B.J. HOSKINS. 1979. On the influence of orography on large-scale atmospheric flow. *J. Atmos. Sci.* **36**: 223–234.

JARRAUD, M.; A.J. SIMMONS and M. KANAMITSU. 1986. Sensitivity of medium range weather forecasts to the use of an envelope orography. European Centre for Medium Range Weather Forecasts, (ECMWF) Rep. No. 56, Reading, England.

KALNAY, E.; K.C. MO and J. PAEGLE. 1986. Large-amplitude, short-scale stationary Rossby waves in the Southern Hemisphere: Observations and mechanistic experiments to determine their origin. *J. Atmos. Sci.* **43**: 252–275.

LAU, N.-C. 1979a. The structure and energetics of transient disturbances in the Northern Hemisphere wintertime circulation. *J. Atmos. Sci.* **36**: 982–995.

———. 1979b. The observed structure of tropospheric stationary waves and local balances of vorticity and heat. *J. Atmos. Sci.* **36**: 996–1016.

———. 1984. Circulation statistics based on FGGE level III-B analyses produced by GFDL. NOAA Data Rep. ERL GFDL-5, Princeton, N.J., 427 pp.

LINDZEN, R.S.; T. ASO and D. JACQMIN. 1982. Linearized calculations of stationary waves in the atmosphere. *J. Meteorol. Soc. Jpn*, **60**: 66–77.

MALONE, R.C.; E.J. PITCHER, M.L. BLACKMON, K. PURI and W. BOURKE. 1984. The simulation of stationary and transient geopotential-height eddies in January and July with a spectral general circulation model. *J. Atmos. Sci.* **41**: 1394–1419.

MECHOSO, C.R. 1981. Topographic influences on the general circulation of the Southern Hemisphere: A numerical experiment. *Mon. Weather Rev.* **109**: 2131–2139.

PALMER, T.N.; G.J. SHUTTS and R. SWINBANK. 1986. Alleviation of a systematic westerly bias in general circulation and numerical weather prediction models through an orographic gravity wave drag parametrization. *Q.J.R. Meteorol. Soc.* **112**: 1001–1039.

SIMMONS, A.J. and B.J. HOSKINS. 1978. The life cycles of some nonlinear baroclinic waves. *J. Atmos. Sci.* **35**: 414–432.

STRAUS, D.M. 1983. On the role of the seasonal cycle. *J. Atmos. Sci.* **40**: 303–313.

———. 1988. The seasonal cycle of energetics from the GLAS/UMD climate GCM. NASA Tech. Memo., NASA/Goddard Space Flight Center, Greenbelt, Md., 44 pp.

——— and J. SHUKLA. 1988. A comparison of a GCM simulation of the seasonal cycle of the atmosphere with observations. Part I: Mean fields and the annual harmonic. ATMOSPHERE-OCEAN, **26**:

TRENBERTH, K.E. 1979. Interannual variability of the 500 mb zonal mean flow in the Southern Hemisphere. *Mon. Weather Rev.* **107**: 1515–1524.

———. 1980. Planetary waves at 500 mb in the Southern Hemisphere. *Mon. Weather Rev.* **108**: 1378–1389.

———. 1982. Seasonality in Southern Hemi-

sphere eddy statistics at 500 mb. *J. Atmos Sci.* **39**: 2507–2520.

———. 1984. Interannual variability of the Southern Hemisphere circulation: Representativeness of the year of the Global Weather Experiment. *Mon. Weather Rev.* **112**: 108–123.

VAN LOON, H. 1972a. Temperature in the Southern Hemisphere. *In:* Meteorology of the Southern Hemisphere, C.W. Newton (Ed.), Meteorol. Monogr. No. 35, Am. Meteorol. Soc., pp. 25–58.

———. 1972b. Pressure in the Southern Hemisphere. Ibid., pp. 59–86.

——— and R.L. JENNE. 1972. The zonal harmonic standing waves in the Southern Hemisphere. *J. Geophys. Res.* **77**: 992–1003.

———; R.L. JENNE and K. LABITZKE. 1973. Zonal harmonic standing waves. *J. Geophys. Res.* **78**: 4463–4471.

ZWIERS, F.W. and G.J. BOER. 1987. A comparison of climates simulated by a general circulation model when run in the annual cycle and perpetual modes. *Mon. Weather Rev.* **115**: 2626–2644.